

# Faint Collimated Herbig-Haro Jets from Visible Stars in L1641

Bo Reipurth<sup>1</sup>, Colin Aspin<sup>1</sup>, John Bally<sup>2</sup>, John J. Tobin<sup>3</sup>, and Josh Walawender<sup>1</sup>

*1: Institute for Astronomy, University of Hawaii at Manoa,  
640 N. Aohoku Place, HI 96720*

reipurth/caa/joshw@ifa.hawaii.edu

*2: Center for Astrophysics and Space Astronomy,  
University of Colorado, Boulder, CO 80309*

John.Bally@colorado.edu

*3: Department of Astronomy, University of Michigan, Ann Arbor, MI 48109*

jjtobin@umich.edu

## ABSTRACT

A population of 11 faint, collimated jets has been discovered in the northern part of the L1641 cloud in the region of HH 1/2, HH 34, and the L1641-N cluster. These jets were missed in previous imaging surveys on account of their weak emission, and they were discovered only on deep exposures with the Subaru 8m telescope. With these new faint jets, the number of HH flows within the area surveyed has doubled. This suggests that collimated jets from young stars may be more common than assumed so far. It is noteworthy that all of the jets are associated with optically visible stars with  $r$ -magnitudes ranging from 13.8 to 22.0. The driving sources of jets in regions flooded by ultraviolet radiation from nearby OB stars are known to be excavated by photo-ionization, and in three cases remnant H $\alpha$  emission envelopes are found associated with the sources, although the more benign environment in the region observed here, about 10 pc distant from the Orion Nebula Cluster, makes the optical visibility of all these sources rather surprising. Such faint jets from visible stars represent either the final vestiges of the outflow phenomenon, or they are triggered by disturbances of the remnant disks, possibly initiated by the orbital evolution of binaries that spiral in to form close binaries. Among the known H $\alpha$  emission stars within the region surveyed, 8% are found to be associated with jets.

*Subject headings:* ISM: jets and outflows stars: formation – stars: pre-main sequence

## 1. Introduction

The northern part of the L1641 cloud is best known for harboring the Orion Nebula Cluster, but also of great interest is the part of the cloud about a degree to the south, where low-mass star formation is abundant. Famous young stars like V380 Ori can be found here (Herbig 1960), as well as the embedded cluster L1641-N (Strom et al. 1989a), together with many dozens of  $H\alpha$  emission stars scattered across the cloud (Haro 1953, Parsamian & Chavira 1982, Wouterloot & Brand 1992, Wiramihardja et al. 1991) and many isolated embedded protostars (Strom et al. 1989b). As a result of this active production of stars, the cloud contains one of the highest known concentrations of Herbig-Haro (HH) flows, including such well-known objects as HH 1/2 (Herbig & Jones 1981) and HH 34 (Reipurth et al. 2002), as well as many molecular outflows (Fukui et al. 1986, Morgan & Bally 1991). A review of the properties of HH flows is given in Reipurth & Bally (2001), and an overview of star formation activity in the L1641 cloud can be found in Allen & Davis (2008). In the following we assume a distance to L1641 similar to that of the ONC, which has been determined to be 414 pc by Menten et al. (2007). For a thorough discussion of distance determinations to the ONC, see Muench et al. (2008).

In this paper, we present a survey for new HH flows in the HH 1/2 and HH 34 region of the L1641 cloud, using a set of very deep images through  $H\alpha$  and [SII] filters obtained at the 8m Subaru telescope. Based on this material we have discovered 11 collimated jets, which are distinguished from the other flows in the region by their weak emission and, in all cases, by emanating from visible stars (Table 1). In Section 2 we give details of the observations, in Section 3 we discuss the individual jets and their driving sources, and in Section 4 we consider the nature of this population of very faint collimated jets.

## 2. Observations

Exposures were made with the 8m Subaru telescope and SuprimeCam. A 5-point dither map with step size of  $40''$  was used in order to cover the  $17''$  gaps between the 10 individual CCDs. An  $H\alpha$  filter was used with a FWHM of  $99 \text{ \AA}$ , central wavelength of  $6596 \text{ \AA}$ , and peak transmission of 87%. The  $H\alpha$  image was obtained in clear conditions on UT Jan 4 2006 with a total exposure time of  $5 \times 12 \text{ min}$  at airmass 1.15, resulting in images with FWHM of  $0.9''$ . A [SII] filter was used with a FWHM of  $130 \text{ \AA}$ , central wavelength of  $6714 \text{ \AA}$ , and peak transmission of 87%. The [SII] image was obtained in clear conditions on UT Jan 5 2006 with a total exposure time of  $5 \times 12 \text{ min}$  at airmass 1.22, and the seeing varied from  $0.61''$  to  $0.65''$  between exposures.

The area surveyed is located in the northern part of the L1641 cloud and covers an area of  $30'$  by  $37'$  approximately centered on the source of the giant HH 34 flow (Fig. 1). Specifically the field ranges in right ascension from 5:34:23 to 5:36:54 and in declination from  $-6:14$  to  $-6:44$  (2000 coordinates).

High-resolution ( $R \sim 35,000$ ) spectra were obtained of the jet-driving sources using the multifiber Hectochelle spectrograph (Szentgyorgyi et al. 1998) on the 6.5m MMT. The chosen echelle order covers the wavelength range of  $\sim 5150$ - $5300$  Å. The spectra were cross-correlated with synthetic stellar spectra, as described in Tobin et al. (2009). Results are listed in Table 2.

Infrared photometry of the jet sources was extracted from the 2MASS catalogue (Skrutskie et al. 2006) and from the Spitzer archive, and optical Sloan photometry (York et al. 2000) was kindly provided by Min Fang (see Fang et al. 2009).

### 3. Results

In the following we describe the individual jets discovered and the known properties of their associated driving sources.

#### 3.1. HH 1020

The HH 1020 jet is a finely collimated bipolar jet with asymmetrical lobes and a total extent of  $134''$  (Fig. 2). The SE lobe is the most extensive, with a length of  $123''$  and consisting of numerous knots of varying brightness along the well defined flow axis at a PA of  $130^\circ$ . These knots are visible in both  $H\alpha$  and [SII], but are brighter in  $H\alpha$ . In contrast, the short NW lobe (with a measurable extent of only  $11''$ ) is primarily emitting in [SII]. It is noteworthy that the jet is perpendicular to the filamentary clouds in the northwestern part of the L1641 clouds.

The source is the  $H\alpha$  emission star Haro 4-222 (Haro 1953) or PaCh 145 (Parsamian & Chavira 1982)<sup>1</sup>, or Kiso 76-103 (Wiramihardja et al. 1991), or WB 406 (Wouterloot & Brand 1992), also known as 2MASS J05343988-0625140. Carpenter et al. (2001) noted its variability in the near-infrared.

---

<sup>1</sup>Parsamian & Chavira (1982) erroneously identify Haro 4-222 = PaCh 145 as the neighboring flare star V766 Ori

Approximately  $20''$  SW of the source one finds the flare star V766 Ori. An optical light curve of V766 Ori is shown by Nicholson & Varley (2006). Our image shows that V766 Ori is actually a small triple system (Figs. 2 and 14) and given the low surface density of stars in this part of L1641 it seems likely that Haro 4-222 forms what might be the 4th star of this small multiple system.

The near-infrared colors of Haro 4-222 (Table 3) indicate a substantial infrared excess. Spitzer clearly detected the source at all wavelengths out to  $24 \mu\text{m}$ . The spectral energy distribution (SED) is shown in Figure 15a. We have used the Robitaille et al. (2006, 2007) models to fit the data, and show our best fit superposed on the data points. The source appears to be a flat-spectrum object, between the Class I and II groups. The color-color diagrams in Figures 16 and 17 reflect this intermediate status. There is, however, one major difference between the observations and the model: the model requires an extensive envelope, which in the models is assumed to be spherically symmetric, and would produce an extinction of  $A_V \sim 7,000$ . Clearly this is not the case, as the source is a visible star, suggesting that the envelope has developed into a flattened structure, allowing us to view the source in the optical.

### 3.2. HH 1021

The HH 1021 jet is very faint, and in addition to the jet the flow contains two faint, more distant, knots. The flow is significantly curved (Fig. 3), with an overall length of  $84''$ . The jet and two knots are visible in both  $\text{H}\alpha$  and  $[\text{SII}]$ , with approximately the same brightness in the two filters. No trace of a counterflow is seen.

The source is a binary, with a companion at a separation of  $3.4''$  and a PA of  $233^\circ$  (Figs. 3 and 14). The jet appears to emanate from the brighter component to the NE.

The source was one of the first variables to be found near the Orion Nebula (Pickering & Leavitt 1904) and is now known as the flare star BW Ori or Parenago 1669 (Parenago 1954). It was found to display  $\text{H}\alpha$  in emission in several surveys and is known as Haro 4-219 (Haro 1953) or PaCh 173 (Parsamian & Chavira 1982) or Kiso 76-118 (Wiramihardja et al. 1991).

The SED of the source seen in Figure 15b and the color-color diagrams in Figures 16 and 17 suggest that the source is a classical T Tauri star with an infrared excess that is modest except at  $24 \mu\text{m}$ .

### 3.3. HH 1022

The HH 1022 jet is the shortest of the flows described in this study, and consists of a single elongated knot at PA  $250^\circ$  reaching a distance of  $5''$  from the source (Fig. 4). The jet is only visible in the [SII] image, indicating that it is of exceptionally low excitation.

The source, which is located just  $2.5'$  west of the prominent HH 34 jet, is known as the  $H\alpha$  emission star Haro 4-224 = PaCh 248 = Kiso 76-153 (Haro 1953, Parsamian & Chavira 1982, Wiramihardja et al. 1991). It is variable in the infrared (Carpenter et al. 2001).

The 2MASS colors indicate that HH 1022 IRS is a Class II source with hardly any reddening or infrared excess, but an excess is detected in the mid-infrared (Figure 15c). The Spitzer colors are consistent with a Class II source (Figures 16 and 17).

### 3.4. HH 1023

The HH 1023 flow is a finely collimated bipolar jet with a total extent of  $16''$ . The NE lobe is shorter ( $5.5''$ ), with well defined knots at a PA of  $64^\circ$ , brighter, and dominant in [SII]. The SW lobe is longer ( $10.5''$ ), substantially fainter, with about the same brightness in  $H\alpha$  and [SII].

The source is a visible star, which is detected in the near-infrared as 2MASS J05355651-0624122. It forms part of a small grouping of stars that includes Haro 4-386, an emission-line star which our images show is a binary with a separation of  $1.3''$  (Fig. 5). Nothing is known about the bright star just north of HH 1023 IRS.

The 2MASS photometry suggests almost no reddening and no near-infrared excess (Figure 15d), but an infrared excess picks up at mid-infrared wavelengths, indicating that HH 1023 IRS may be surrounded by a disk with an inner gap. The model shown assumes an envelope with high extinction, so this is another case where the envelope clearly cannot be spherical. The position of HH 1023 IRS in color-color diagrams suggests that it is a border-line Class I source (Figs. 16 and 17).

### 3.5. HH 1024

The HH 1024 flow is highly asymmetric, with a faint, collimated northern lobe about  $33''$  in extent at a PA of  $6^\circ$ , and a southern lobe that consists of a single, large and bright knot,  $4''$  from the source. The northern lobe shows distinct wiggling (Fig. 6).

The source is an anonymous star, which has not drawn any previous attention. It is among the optically faintest of the stars discussed here. The 2MASS colors do not indicate much near-infrared excess, and the IRAC-photometry suggests a Class II source (Figure 16), but a strong excess is seen at  $24\ \mu\text{m}$ , which suggests a Class I source (Figure 17). The overall SED in Figure 15e indicates a significant envelope, which must be flattened in order for the star to be visible.

### 3.6. HH 1025

The HH 1025 jet is a finely collimated bipolar jet located just west of the bright Herbig-Haro object HH 3 (for a general view of the region, see Reipurth 1985). The NE lobe is shorter, with a total extent of  $25''$ , starting out at a PA of  $36^\circ$ , but after  $13''$  the jet shows a distinct bend in the flow axis. The SW lobe is perfectly straight and much longer, totaling an extent of  $65''$  (Fig. 7).

The driving source is the well known variable star AV Ori (HBC 159 = Haro 4-236 = Parenago 2312), which has a fainter companion  $5.9''$  to the NW at a PA of  $303^\circ$ , called AV Ori/c by Cohen & Kuhi (1979), who found it to be an emission line star; the companion is also known as HBC 481 (Herbig & Bell 1988). The irregular variability of AV Ori has been documented by Wolf (1903), Pickering & Leavitt (1904), and Grankin et al. (2007), among others. AV Ori was detected in surveys for  $H\alpha$  emission line stars by Haro (1953), Wiramihardja et al. (1991), and Wouterloot & Brand (1992). Low-dispersion spectroscopy by Cohen & Kuhi (1979) suggests a spectral type of K4e, and Allen (1995) lists it as K5. The star was also detected in X-rays by Pravdo & Angelini (1993). Using 2MASS and Spitzer photometry, Fang et al. (2009) determined a luminosity (their source #56) of  $3.8 L_\odot$  and an extinction of 2.2 magnitudes. The SED in Figure 15f suggests a modest infrared excess mainly at longer wavelengths. The star is evidently a Class II source (Figures 16 and 17).

### 3.7. HH 1026

The HH 1026 jet is a highly collimated flow with a total extent of  $128''$  (Fig. 8). A few very faint knots extend on either side of the driving source. The northern lobe terminates in a faint bow shock  $46''$  from the source. A group of faint anonymous HH knots resembling an extended bow shock are located about 3 arcmin north of the source along the flow axis, but it is unclear whether they are related to the HH 1026 flow. The southern lobe, in contrast, displays a bright segment  $10''$  long starting  $53''$  from the source, and terminates in a bow

shock  $105''$  from the source. The driving source, which is among the optically faintest of the sources discussed here, shows elongation in the direction of the flow, but other than that nothing is known about it, it has not drawn any attention in any other survey, in particular it is not included in the 2MASS catalogue. The nearest 2MASS source is J05360665-0632171, which is a bright ( $r \sim 15.2$ ) visible star  $53''$  to the SE.

The available optical and Spitzer photometry shows a rising SED (Figure 15*g*), and the Spitzer colors (Figures 16 and 17) are consistent with a Class I source with a significant envelope. Again, the optical visibility, although faint, suggests that the envelope is flattened.

### 3.8. HH 1027

The HH 1027 jet is a well collimated flow, albeit asymmetric and somewhat perturbed (Fig. 9). It is seen only in [SII], and has a total extent of  $2.5'$ , with a northern irregular lobe extending over  $22''$ , and a southern slightly curved lobe extending  $128''$ . The source is optically faint, but is weakly detected in the near-infrared as 2MASS J05361960-0636171.

The SED of the driving source shows no evidence for circumstellar material (Figure 15*h*). This is the only one among the 11 jet sources discussed here that is not detected at  $24 \mu\text{m}$ . The Spitzer IRAC colors are consistent with a Class III source. It is noteworthy that the referee of this paper has found two fan-shaped cavities in deep  $\text{H}_2$  images close to, but not exactly on, the axis of the poorly defined southern end of the HH 1027 jet. Further work is required to determine whether this could be evidence for an alternative jet source, or it is an unrelated young star.

### 3.9. HH 1028

The HH 1028 jet has a single well collimated lobe with many faint (primarily  $\text{H}\alpha$  emitting) knots extending  $58''$  to the SW at a PA of  $231^\circ$ , where two bright [SII]-dominant knots are located (Fig. 10). More knots are found further to the SW, but not precisely on the flow axis, so their provenance is unknown (see Fig. 11). The flow is located in the outskirts of the embedded L1641-N cluster, and is driven by the variable star V584 Ori. Hodapp & Deane (1993) obtained an infrared spectrum of the star (their source #45), showing weak absorption lines of Na, Ca, and CO, indicating a spectral type of K5. No  $\text{Br}\gamma$  absorption was seen. Galfalk & Olofsson (2008) suggest a spectral type of K6, and Allen (1995) suggests M0.5, both from optical spectroscopy. The star is listed as Haro 4-214 = PaCh 401 = Kiso 76-268 in the  $\text{H}\alpha$  emission star catalogues of Haro (1953), Parsamian & Chavira

(1982), and Wiramihardja et al. (1991), respectively. Fang et al. (2009) classifies the star (their source #118) as a weak-line T Tauri star. V584 Ori was included in the large infrared variability survey of Carpenter et al. (2001).

The 2MASS colors indicate a significant infrared excess, and the SED shows that this extends into the mid-infrared (Figure 15*i*). The Spitzer colors are consistent with a Class II source (Figures 16 and 17).

### 3.10. HH 1029

The HH 1029 flow is a finely collimated jet stretching across 2 arcmin (Fig. 11). It is already known at infrared wavelengths, where it consists of two faint H<sub>2</sub> emission knots (these are called SMZ 5-20 and 5-22 in Stanke et al. 1998, their Figure 1). The infrared flow is labeled as SMZ 54 in Stanke, McCaughrean, Zinnecker (2002), and is also seen in the H<sub>2</sub> images of Galfalk & Olofsson (2007). In the optical the flow is pointing straight back to a nebulous star, variously known as Haro 4-403 (Parsamian & Chavira 1982), Re 40 (Reipurth 1985), and Kiso 76-258 (Wiramihardja et al. 1991). No other source is found along the flow axis in the Spitzer images of this region. The insert in Figure 11 shows that the star is faintly visible at optical wavelengths, and is surrounded by a large disk shadow, suggesting that the disk is nearly edge-on. The flow is at a position angle of 132°, which is perpendicular to the disk shadow. Close to the star two very faint and highly collimated jets are seen emanating from the bipolar reflection nebula, the one to the SE is more pronounced and seen in both the H $\alpha$  and [SII] images, whereas the one to the NW is only barely visible in the [SII] image.

If one follows the well defined flow axis of the HH 1029 flow from the source to the NW one comes to an already known object, HH 298A (Reipurth et al. 1998a), located along the flow axis and at the same distance to the source as the first bright knot in the HH 1029 jet. This strongly suggests that HH 298A is a part of the counterflow to HH 1029. Two fainter, diffuse knots (HH 298B and C) are found to the east of HH 298A, not on the well-defined flow axis; in view of the likely association between HH 298A and HH 1029, it is unclear whether the knots B and C are related to A. The total extent of the HH 298/HH 1029 flow is about 366 arcsec, which at the assumed distance of 414 pc corresponds to about 0.75 pc, making this flow the largest of the 11 jets discussed in this paper.

The SED of the source shows an infrared excess, especially at 24  $\mu$ m (Figure 15*j*). The Spitzer colors suggest that the star is a Class II source (Figures 16 and 17).

### 3.11. HH 1030

The HH 1030 flow is a highly collimated bipolar jet, with a prominent southern lobe containing dozens of closely spaced knots that stretches over  $67''$ . The northern lobe is less distinct and terminates in an isolated bow shock  $90''$  from the source (Fig. 12). The two lobes deviate from a common straight line. Whereas the northern lobe is brighter in  $H\alpha$ , the southern lobe is dominant in [SII]. At the location of the brightest knot, the southern lobe slightly changes direction; we cannot exclude the possibility that this could be a separate flow with an as yet unidentified source.

The source is the variable star V585 Ori that is also an  $H\alpha$  emission line star known as Haro 4-227 = PaCh 410 = Kiso 76-274 (Haro 1953, Parsamian & Chavira 1982, Wiramihardja et al. 1991). Allen (1995) suggests a spectral type of K8. Fang et al. (2009) classifies the star (their object #131) as a classical T Tauri star with an extinction of 3.9 magnitudes. Our images show a companion at a separation of  $4.3''$  in PA  $202^\circ$  (Figs. 12 and 14). Our Hectochelle spectrum of the 5150–5300 Å region shows a rich emission line spectrum (Fig. 13), with the following rather prominent lines (a colon indicates a probable classification).

FeII 5169.85 (42) (blended with MgI 5167.32/5172.68 (2):)

MgI 5183.60 (2):

FeII 5197.57 (49)

FeII 5234.62 (49)

CaI 5270.27 (22):

FeII 5275.99 (49)

FeII 5284.09 (41)

Comparison with high-resolution spectra of active T Tauri stars kindly provided by George H. Herbig shows that this spectral region is often rich in emission lines of iron, but with greatly varying strengths and ratios depending on the temperature of the line emitting region. The emission spectrum of V585 Ori shows a remarkable similarity to that of DG Tau, which is also known to drive a collimated jet (e.g. Bacciotti et al. 2000).

The 2MASS photometry indicates a substantial infrared excess, which continues into the mid-infrared (Figure 15*k*). The Spitzer colors are consistent with the star being a Class II source (Figures 16 and 17).

## 4. Discussion

### 4.1. Statistics of HH Jets in L1641

The rich population of HH flows in the northern part of L1641 offers an opportunity to do some statistical estimates of the frequency of HH flows. Within the Subaru image a number of HH flows are already known. Several of these are giant, parsec-scale flows, and as flows that were previously assumed to be independent are found to belong as components of a giant flow, the number of HH flows in the region has diminished. Examples are the well collimated HH 33/40 and HH 85 flows, which are now seen merely as part of the giant HH 34 jet complex. We have counted the number of independent HH flows in the Subaru field, and find 8 flows that either have well defined driving sources, or cannot be associated with a known giant flow. These flows are 1) the giant HH 34 jet complex (including HH 33/40, 85, 86, 87, 88, 327), 2) the giant HH 401 bow shock associated with HH 1/2/3, 3) the giant HH 35/HH 222 flow from V380 Ori, and 4-8) a group of HH flows emanating from sources in the L1641-N cluster: HH 299, HH 301/302, HH 303, HH 304, and HH 305. A number of faint additional HH shocks are found in the Subaru images, but most or all are likely to belong to one of the various giant HH flows crossing the region, although we cannot exclude the possibility that future proper motion studies will reveal additional independent flows.

Unless the L1641 region is somehow atypical, the discovery of 11 new, faint HH jets indicates that HH flows may be significantly more common, by a factor of about 2, than hitherto assumed.

### 4.2. Nature and Origin of the Driving Sources

Whereas the driving sources of the 8 previously known HH flows within the Subaru field are mostly embedded infrared sources without optical counterparts, all of the 11 new flow sources are visible stars.

Robitaille et al. (2007) have presented a large set of star/disk/envelope models, which we used in Section 3 to characterize the environment of the individual sources<sup>2</sup>. All the sources have one thing in common, namely that they are visible in the optical, ranging from bright ( $r \sim 13.8$ ) to faint ( $r \sim 22.0$ ). But the SEDs and the locations in color-color diagrams reveal a wide range in circumstellar properties of the sources, from Class I sources to Class III

---

<sup>2</sup>These models were derived using the spectral energy distribution fitting tool at <http://caravan.astro.wisc.edu/protostars/>

sources. In the following we attempt to understand this range of properties.

It is well known that some visible T Tauri stars are associated with HH jets, which in certain cases can be quite bright. Examples include RW Aur (Melnikov et al. 2009), DG Tau (Bacciotti et al. 2000), HL Tau (Mundt et al. 1990), and V510 Ori (Reipurth et al. 1998b).

There are in principle three ways for a T Tauri star to transit from an embedded infrared source to an optically visible star. First, it may excavate itself through its outflow activity, blowing away the remnants of its nascent cloud core (Lada & Shu 1990). Second, the star may be flung away from its core by dynamical interactions in a small multiple system (Reipurth 2000). And third, the environment of the star may be ablated by the presence of a nearby OB star (Reipurth et al. 1998b).

The region of the L1641 cloud that we are focusing on here is far removed from the OB stars at the center of the Orion Nebula Cluster, so they are likely to be affected by only a rather benign ultraviolet radiation field. This leaves the other two possibilities to explain the visibility of all these jet sources.

In favor of the first case, we note that at the end of the outflow phase the sources are much more likely to be visible than earlier, because the infalling envelope is close to being depleted and the cavity dug by the outflow activity may have gradually widened. Also, the very low surface brightness of the new jets suggests weak shocks, which conceivably could be related to a decline in the functioning or feeding of the jet engine. Finally, the fact that almost all of the jet sources have substantial infrared excesses could indicate that they are less evolved than the average visible T Tauri star in the region. In short, the discovery of a population of visible stars with very faint jets can be reconciled with our current view of the evolution of young stars.

The second case, however, also has appealing aspects. We note that some of the sources discussed here have spectral energy distributions typical of Class I sources, which are generally not optically visible, but may become visible in the following manner. Triple and higher-order multiple systems are born in a non-hierarchical configuration, and dynamically evolve into a hierarchical form through close interactions. Usually it is the lightest component that is ejected into a distant orbit or is altogether freed. The remaining pair forms a new binary, and because the binary frequently has a high eccentricity, it evolves viscously as the circumstellar material of the components interact. During the increasingly close and increasingly frequent periastron passages, accretion is enhanced, leading to outflow activity. Herbig-Haro jets thus can be interpreted as the fossil record of the early evolution of a new-born binary (Reipurth 2000). If interpreted within this scenario, the 11 jet sources should be

unresolved close binaries ( $\sim 10$  AU), and in addition to the above processes, their visibility may be aided by the binary recoiling out of its cloud core by the dynamical interactions with a third component. This third component may be in a bound orbit less than a few hundred AU in size, and thus only visible through adaptive optics observations. Or it may be in a larger orbit, and resolvable with our images. We note that four of the 11 sources are associated with a visible companion or multiple system. Finally, in some cases the ejection event may have led to an unbound system and the third component may have left the system. A more detailed study of the 11 driving sources is required to cast light on whether such dynamical interactions have perhaps aided some of them, in particular the Class I sources, to become visible.

### 4.3. How Common are Jets during the T Tauri stage?

We now estimate what fraction of visible T Tauri stars are associated with HH jets. The  $30' \times 37'$  region in northern L1641 imaged with the Subaru telescope for this study is fully covered by the major, deep survey for  $H\alpha$  emission stars by Pettersson, Armond, & Reipurth (2011). Their list contains 99  $H\alpha$  emission stars within that field. All 11 new jets have well identified visible driving sources and among those, 7 are included in the Pettersson et al. catalog (the rest presumably being fainter than the detection limit of the Pettersson et al. survey). One more of the 99 stars of Peterson et al. is associated with a jet, HH 305, namely a fainter companion to the young variable PR Ori (Reipurth et al. 1998a, also see Fig. 1). Altogether, it appears that  $\sim 8\%$  of visible  $H\alpha$  emitters have jets at any given time. In other words, the presence of a physically resolved jet (as opposed to being associated with unresolved shocked emission) occurs only for a very small subset of young visible stars at any given time. This is consistent with the general finding that most jet energy sources are still deeply embedded in their placental material and thus detectable only as infrared sources.

### 4.4. $H\alpha$ Envelopes in Northern L1641

Three of the jet sources discussed here have small, faint envelopes visible only in  $H\alpha$  but not in [SII], indicating that these are not simply compact reflection nebulae. We have searched for further of these  $H\alpha$  envelopes around other stars in this field and have found a total of eight such objects, which are listed in Table 4.

All of these objects are on the western side of the Subaru image and have similar surface brightness in  $H\alpha$ . Several of these objects (No. 1 - Haro 4-222 / HH 1020 and No.

2 - BW Ori / HH 1021) are located more than a parsec west of the western edge of the Orion A molecular cloud in a region nearly devoid of molecular gas. The H $\alpha$  emission is limb-brightened in several of the objects, including No. 1 and No. 8 and possibly No. 5. The central stars tend to be located towards the north rim of the envelopes. The radii of these objects range from about 2'' to 8'' ( $\sim$ 800 to 3200 AU).

The relatively similar surface brightness, limb-brightening, location on the western side of the Orion A molecular cloud, and displacement of the central stars towards the north suggest that the H $\alpha$  emission traces ionization fronts surrounding compact neutral globules containing young stars. These objects have dimensions comparable to the largest proplyds observed in the outskirts of the Orion Nebula such as the "Beehive Proplyd" (Bally et al. 2005, Smith et al. 2005). They may be exposed to the ionizing Lyman continuum radiation which permeates the interior of the Orion super-bubble and which ionizes Barnard's Loop in the east and the Eridanus Loop in the west (see Bally 2008 for an overview). Some of this radiation may originate from massive stars in the Orion Nebula that escapes along density-bounded portions of the nebula; the rest may come from massive stars distributed in the extended OB association.

Nearly one-half of the stars with such H $\alpha$  envelopes power outflows. The envelopes indicate the presence of extended reservoirs of gas surrounding these young stars. However, only about 5% of the young stars in the region under study exhibit H $\alpha$  envelopes.

These envelopes may trace circumstellar material that has survived until now despite being in an ionizing environment. A crude estimate of the expected mass-loss rate due to photo-ablation can be obtained by assuming that a spherical cloud of radius  $r$  is illuminated by a Lyman continuum radiation field of luminosity  $Q$  at a distance  $D$ . It is assumed that the cloud is sufficiently dense to remain neutral and that its gas is stationary. Assume that at the cloud surface, photo-ablated gas is accelerated to a constant speed  $C \approx 10 \text{ km s}^{-1}$  by the heating effect of the ionizing radiation and that in the steady state, the flow forms a spherically divergent wind with  $\dot{M} = f\pi r^2 \mu m_H n(r) C$  where  $f$  is a geometric factor close to one,  $\mu$  is the mean molecular weight,  $m_H$  is the mass of hydrogen, and  $n(r)$  is the number density in the flow at radius  $r$ . The density in such a wind decreases as  $n(r) = n(r_I)(r_I/r)^2$  where  $r_I$  is the radius of the ionization front (e.g. the radius of the dense and neutral cloud) and  $n(r_I)$  is the electron density just outside this front after it has been accelerated to a velocity  $C$ . This electron density is regulated by recombinations occurring within the diverging ionized wind ablating from the cloud. Integrating the recombination rate per unit volume,  $n^2(r)\alpha_B$ , from the ionization front to infinity, setting this equal to the ionizing flux, and solving for the electron density at the front gives  $n_e(r_I) = (3Q/4\pi\alpha_B r_I)^{1/2} 1/D$ . Here,  $\alpha_B = 2.6 \times 10^{-13}$  is the case-B recombination coefficient for hydrogen.

For  $Q = 10^{49}$  ionizing photons per second and assuming  $D = 10$  pc (the Orion Nebula is located at a projected distance of about 6 to 7 pc north of this field), and adopting  $r = 3 \times 10^{16}$  cm, one derives an electron density just outside of the ionization front of  $n_e \approx 600 \text{ cm}^{-3}$ . The resulting peak emission measure is  $EM = \int n_e^2 dl \approx 3 \times 10^3 \text{ cm}^{-6} \text{ pc}$  (which arises at the projected edge of the cloud), corresponding to a peak  $H\alpha$  surface brightness of  $I(H\alpha) = 7 \times 10^{-15} \text{ erg s}^{-1} \text{ cm}^{-2} \text{ arcsec}^{-2}$ . This is an upper bound since only attenuation of Lyman continuum by photo-ablation flow from the cloud has been considered; other dust or gas between the UV source and the cloud has been ignored. Furthermore, foreground dust will also diminish the  $H\alpha$  surface brightness. These numbers are consistent with the observed brightness of the objects in the images. The resulting mass loss-rate is  $\dot{M} \approx \pi r^2 \mu m_H n_e C \approx 8 \times 10^{-8} M_\odot \text{ yr}^{-1}$ . At this radius, a  $0.1 M_\odot$  clump could survive for about  $10^6$  years.

Alternatively, the envelopes may have recently been dynamically ejected from a much smaller but denser region surrounding the star. More compact and denser reservoirs can survive longer since they lose mass to photo-ablation at a lower rate. A dynamical event in the inner disk such as an interaction with a companion star, or even a giant planet, may expel some mass to radii of order a few thousand AU where it can be photo-ablated and easily resolved on ground-based images.

The  $H\alpha$  envelopes may either trace the relatively rare YSOs that have retained envelopes for an unusually long time of order a few Myr, or trace relatively rare phenomena in the lives of forming stars. Either way, extended circumstellar envelopes may indicate ongoing late-phase accretion and jet production.

#### 4.5. Orientation of Jets

The position angles of the axes of the new jets appear as a whole to be randomly oriented. But within one area of the cloud, the northwestern part, there could be an alignment. The HH 1020 and HH 1021 flows are both directed towards the NW, as is the HH 83 jet located further west and just outside the Subaru image. The axis of symmetry of the giant bow shock HH 401, associated with the HH 1/2 complex and prominently visible in Fig. 1, is also aligned with these flows (Ogura 1995).

Reipurth (1989) drew attention to the fact that the northwestern part of the L1641 cloud has a streaky structure, with long parallel filaments or sheets of apparently tenuous gas photoionized by the general UV radiation field from the Orion Nebula Cluster (see Fig. 1). Such structures do not appear to exist in other parts of the L1641 cloud. The filaments are approximately oriented perpendicular to the outflow direction of the abovementioned

jets. Heyer et al. (1987) noted that the polarization vectors of background stars, and thus presumably the magnetic field, is oriented in a NW-SE direction. While the evidence for an alignment between outflows and the local magnetic field is controversial, at least in the case of this part of the L1641 cloud, there might be a link.

Hartmann, Calvet, & Boss (1996) considered the collapse of cores in sheets of gas, and Hartmann & Burkert (2007) examined the development of filaments in the Orion A cloud. It is possible that in the filamentary or sheet-like structures in the northwestern part of L1641 we see examples of such collapse of sheets along magnetic field lines, resulting in disks oriented perpendicular to the magnetic field, and thus outflows parallel to the magnetic field.

#### 4.6. Kinematics of Jet Sources

We have observed most of the new jet sources with the Hectochelle spectrograph at the 6.5m MMT, see Section 2. Of these, six sources had a high enough cross correlation parameter to determine a stellar radial velocity. Table 2 lists the resulting heliocentric velocities. These values should be compared to the heliocentric velocity of the Orion Nebula Cluster, which is about 26 km/s with a velocity dispersion of about 3 km/s (Furesz et al. 2008). For HH 1030 IRS = V585 Ori only emission lines are seen in the echelle order observed, so the velocity listed is measured from these. In all cases but one, the velocities are within  $3\sigma$  of the velocity of the ONC. The exception is HH 1020 IRS = Haro 4-222, which is possibly a spectroscopic binary.

### 5. Conclusions

We have analyzed very deep interference filter  $H\alpha$  and [SII] images, obtained with the 8m Subaru telescope under excellent seeing conditions, of the northern part of the L1641 cloud harboring the HH 34 and HH 222 giant HH flows and the L1641-N cluster, and the following results were obtained:

1. Eleven very faint and highly collimated jets, HH 1020 to HH 1030, have been discovered to emanate from visible young stars. About 8 distinct HH flows with identifiable driving sources were known within this region prior to the present study, suggesting the possibility that HH flows in star forming regions could be twice as common as previously anticipated.

2. The field of view observed harbors 99 stars identified in a recent homogeneous survey for  $H\alpha$  emission stars, and 7 of the new jet sources are found among these. One more of these  $H\alpha$  emitters drives a previously known HH flow. Overall, therefore, 8% of the T Tauri

stars associated with the northern L1641 molecular cloud are found to currently drive jets.

3. The eleven sources have one thing in common, namely that they are all optically visible, ranging in brightness from  $r$  of 13.8 to 22.0. But in terms of their circumstellar environment the sources span a considerable range, from Class I to Class III sources.

4. The sources may be visible stars because their envelopes have become depleted and their outflow activity have carved cavities that expose the driving sources to view. However, some of the sources have spectral energy distributions that classify them as Class I sources, and we speculate that they have been prematurely exposed to view by dynamical interactions in triple or small multiple systems.

5. Three of the jet sources are surrounded by faint  $H\alpha$  emission envelopes. Another five stars are found associated with similar envelopes. These may be remnants of the original infalling envelopes which have survived until now, or they may be circumstellar material that has been truncated and torn away in dynamical interactions.

6. We note that these jets and their sources may be of particular interest for detailed studies of the jet engine, similar to those of, e.g., Andrews et al. (2004) and Melnikov et al. (2009), due to their limited obscuration of the jet acceleration region.

Thanks are due to the Subaru staff, in particular Miki Ishii and Hisanori Furusawa, for excellent and dedicated support during the observations. We are grateful to Nobunari Kashikawa for permission to use his [SII] filter, to Min Fang for providing the optical photometry, and to George Herbig and an anonymous referee for valuable comments. We have benefited from the use of the spectral energy distribution fitting tool at <http://caravan.astro.wisc.edu/protostars>. Based in part on data collected at the Subaru Telescope, which is operated by the National Astronomical Observatory of Japan (NAOJ). This work is based in part on observations made with the Spitzer Space Telescope, which is operated by the Jet Propulsion Laboratory, California Institute of Technology under a contract with NASA. This publication makes use of data products from the Two Micron All Sky Survey, which is a joint project of the University of Massachusetts and the Infrared Processing and Analysis Center/California Institute of Technology, funded by the National Aeronautics and Space Administration and the National Science Foundation. This work was supported by NSF grant AST-0407005, and by the National Aeronautics and Space Administration through the NASA Astrobiology Institute under Cooperative Agreement No. NNA08DA77A issued through the Office of Space Science. JJT acknowledges support from grant HST-GO-11548.04-A. This research has made use of the SIMBAD database, operated at CDS, Strasbourg, France, and of NASA's Astrophysics Data System Bibliographic Services.

## REFERENCES

- Allen, L.E. 1995, PhD thesis, School of Physics, University of New South Wales, Sydney, Australia
- Allen, L.E. & Davis, C.J. 2008, in *Handbook of Star Forming Regions*, Vol. I, ed. Bo Reipurth, Astron. Soc. Pacific, p.621
- Allen, L.E., Calvet, N., D’Alessio, P., Merin, B., Hartmann, L. et al. 2004, *ApJS*, 154, 363
- Andrews, S.M., Reipurth, B., Bally, J., Heathcote, S.R. 2004, *ApJ*, 606, 353
- Bacciotti, F., Mundt, R., Ray, T.P., Eisloffel, J., Solf, J., & Camenzind, M. 2000, *ApJ*, 537, L49
- Bally, J., Licht, D., Smith, N., & Walawender, J. 2005, *AJ*, 129, 355
- Bally, J. 2008, in *Handbook of Star Forming Regions*, Vol.I, ed. Bo Reipurth, Astron. Soc. Pacific, p. 459
- Balog, Z., Muzerolle, J., Rieke, G.H., Su, K.Y.L., Young, E.T., & Megeath, S.T. 2007, *ApJ*, 660, 1532
- Carpenter, J.M., Hillenbrand, L.A., & Skrutskie, M.F. 2001, *AJ*, 121, 3160
- Cohen, M. & Kuhi, L.V. 1979, *ApJS*, 41, 743
- Fang, M., van Boekel, R., Wang, W., Carmona, A., Sicilia-Aguilar, A., & Henning, Th. 2009, *A&A*, 504, 461
- Fukui, Y., Sugitani, K., Takaba, H., Iwata, T., Mizuno, A., Ogawa, H., & Kawabata, K. 1986, *ApJ*, 311, L85
- Furesz, G., Hartmann, L.W., Megeath, S.T., Szentgyorgyi, A.H., & Hamden, E.T. 2008, *ApJ*, 676, 1109
- Galfalk, M. & Olofsson, G. 2007, *A&A*, 466, 579
- Galfalk, M. & Olofsson, G. 2008, *A&A*, 489, 1409
- Grankin, K.N., Melnikov, S.Y., Bouvier, J., Herbst, W., & Shevchenko, V.S. 2007, *A&A*, 461, 183
- Haro, G. 1953, *ApJ*, 117, 73

- Hartmann, L. & Burkert, A. 2007, ApJ, 654, 988
- Hartmann, L., Calvet, N., & Boss, A. 1996, ApJ, 464, 387
- Herbig, G.H. 1960, ApJS, 4, 337
- Herbig, G.H. & Jones, B.F. 1981, AJ, 86, 1232
- Herbig, G.H. & Bell, K.R. 1988, Lick Obs. Bull. No. 1111
- Heyer, M.H., Strom, S.E., & Strom, K.M. 1987, AJ, 94, 1653
- Hodapp, K.W. & Deane, J. 1993, ApJS, 88, 119
- Lada, C.J. & Shu, F.H. 1990, Science, 248, 564
- Melnikov, S., Eislöffel, J., Bacciotti, F., Woitas, J., & Ray, T.P. 2009, A&A, 506, 763
- Menten, K.M., Reid, M.J., Forbrich, J., & Brunthaler, A. 2007, A&A, 474, 515
- Morgan, J.A. & Bally, J. 1991, ApJ, 372, 505
- Muench, A., Getman, K., Hillenbrand, L., & Preibisch, T. 2008, in *Handbook of Star Forming Regions*, Vol. 1, Ed. Bo Reipurth, Astron. Soc. Pacific, p. 483
- Mundt, R., Bührke, T., Solf, J., Ray, T.P. & Raga, A.C. 1990, A&A, 232, 37
- Nicholson, M. & Varley, H. 2006, Open European Journal on Variable Stars, 17, 1
- Parsamian, E.S. & Chavira, E. 1982, Bol. Inst. Tonantzintla, 3, 69
- Pettersson, B., Armond, T., & Reipurth, B. 2011, in preparation
- Pickering, E.C. & Leavitt, H.S. 1904, ApJ, 19, 289
- Pravdo, S.H. & Angelini, L. 1993, ApJ, 407, 232
- Reipurth, B. 1985, A&AS, 61, 319
- Reipurth, B. 1989, A&A, 220, 249
- Reipurth, B. 2000, AJ, 120, 3177
- Reipurth, B. & Bally, J. 2001, Ann. Rev. Astron. Astrophys., 39, 403
- Reipurth, B., Devine, D., & Bally, J. 1998a, AJ, 116, 1396

- Reipurth, B., Bally, J., Fesen, R.A., & Devine, D. 1998b, *Nature*, 396, 343
- Reipurth, B., Heathcote, S., Morse, J., Hartigan, P., Bally, J. 2002, *AJ*, 123, 362
- Robitaille, T.P., Whitney, B.A., Indebetouw, R., Wood, K., & Denzmore, P. 2006, *ApJS*, 167, 256
- Robitaille, T.P., Whitney, B.A., Indebetouw, R., & Wood, K. 2007, *ApJS*, 169, 328
- Skrutskie, M.F., Cutri, R.M., Stiening, R., Weinberg, M.D., Schneider, S. et al. 2006, *AJ*, 131, 1163
- Smith, N., Bally, J., Licht, D., & Walawender, J. 2005, *AJ*, 129, 382
- Stanke, T., McCaughrean, M.J., Zinnecker, H. 1998, *A&A*, 332, 307
- Stanke, T., McCaughrean, M.J., Zinnecker, H. 2002, *A&A*, 392, 239
- Strom, K.M., Margulis, M., & Strom, S.E. 1989a, *ApJ*, 346, L33
- Strom, K.M., Newton, G., Strom, S.E., Seaman, R.L., Carrasco, L., Cruz-Gonzalez, I. et al. 1989b, *ApJS*, 71, 183
- Szentgyorgyi, A.H., Cheimets, P., Eng, R., Fabricant, D.G., Geary, J.C. et al. 1998, *Proc. SPIE*, 3355, 242
- Tobin, J.J., Hartmann, L., Furesz, G., Mateo, M., Megeath, S.T. 2009, *ApJ*, 697, 1103
- Wiramihardja, S.D., Kogure, T., Yoshida, S., Nakano, M., Ogura, K., & Iwata, T. 1991, *PASJ*, 43, 27
- Wolf, M. 1903, *AN*, 163, 161
- Wouterloot, J.G.A. & Brand, J. 1992, *A&A*, 265, 144
- York, D.G., Adelman, J., Anderson, J.E., Jr., Anderson, S.F., Annis, J. et al. 2000, *AJ*, 120, 1579

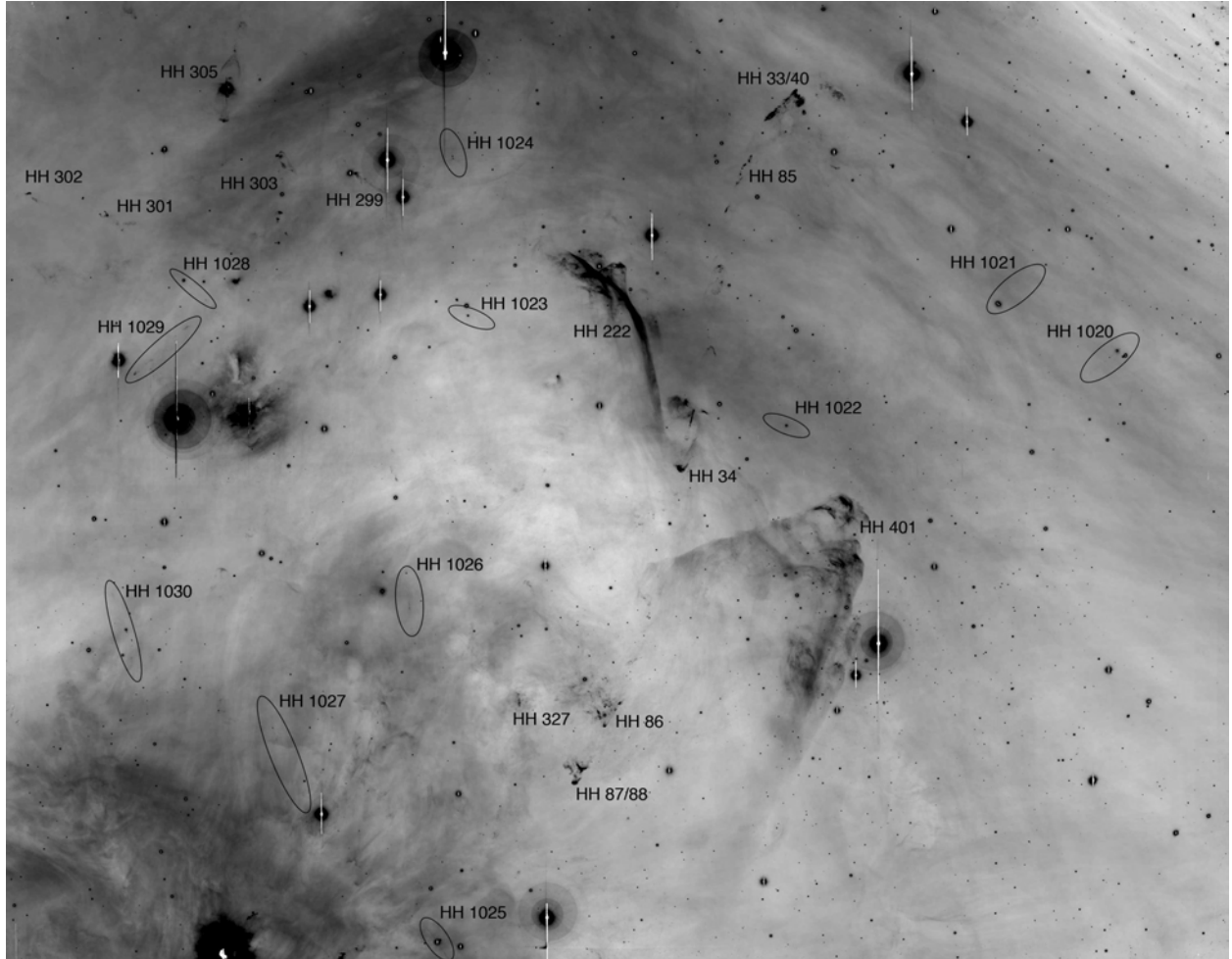


Fig. 1.— An overview of the entire field of northern L1641 imaged with the Subaru telescope. The new flows HH 1020–1030 are marked with ellipses; other HH flows referred to in the text are also labeled. The figure is a combination of an  $H\alpha$  and a  $[SII]$  image, and covers approximately  $30' \times 37'$ . North is up and east is left.

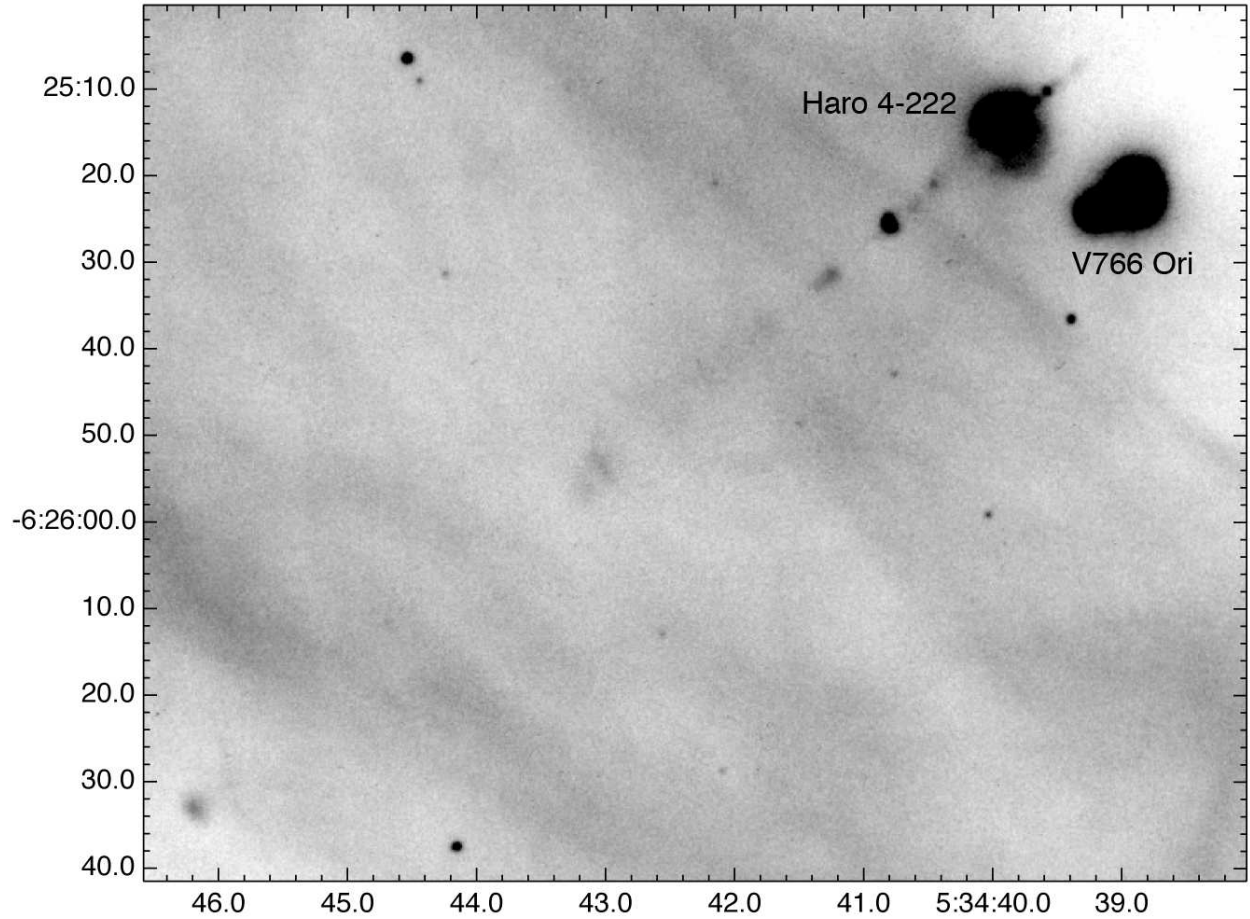


Fig. 2.— The HH 1020 jet emanating from Haro 4-222 as seen in an  $H\alpha+[SII]$  image from the Subaru 8m telescope. It forms a small clustering together with the flare star V766 Ori, which we resolve into a close triple system.

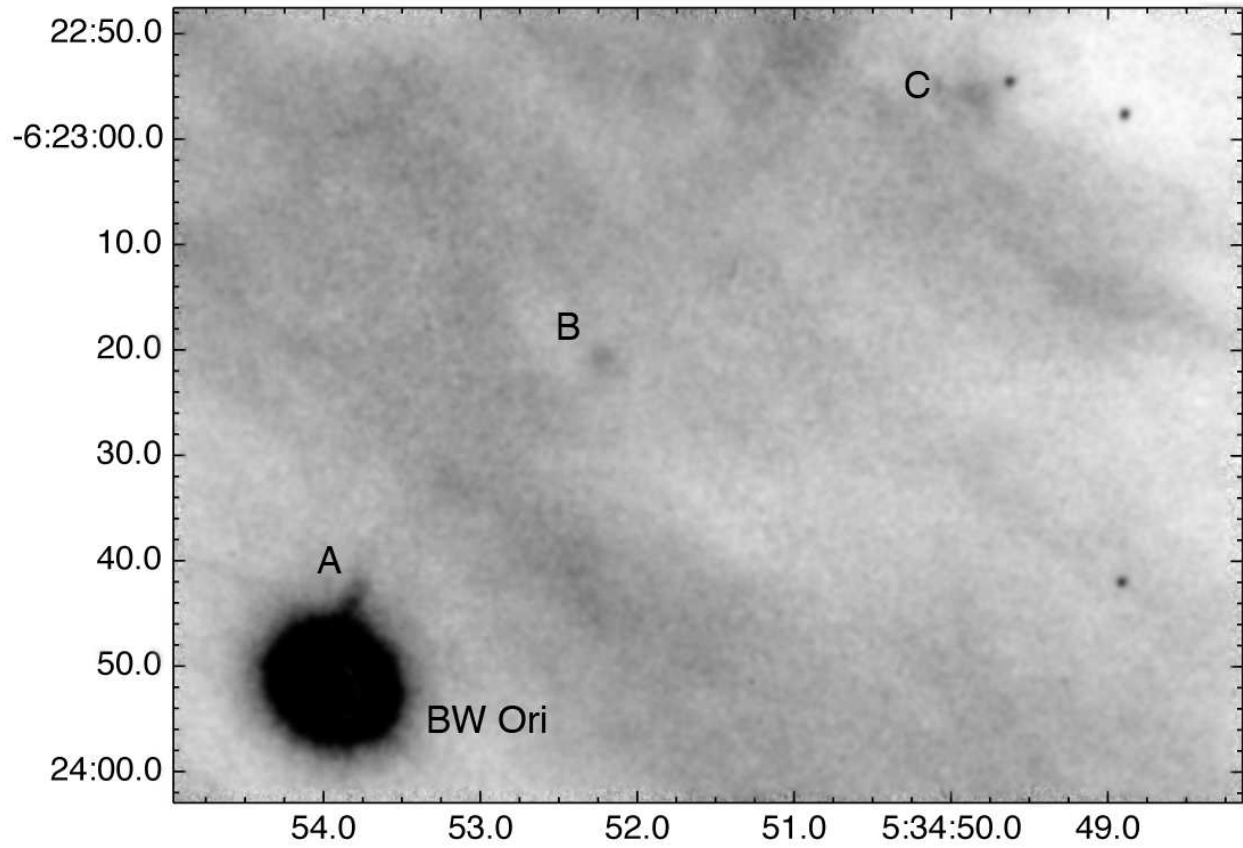


Fig. 3.— The HH 1021 jet emanating from the NE component of the binary 2MASS J05345404-0623507 as seen in a [SII] image from the Subaru 8m telescope.

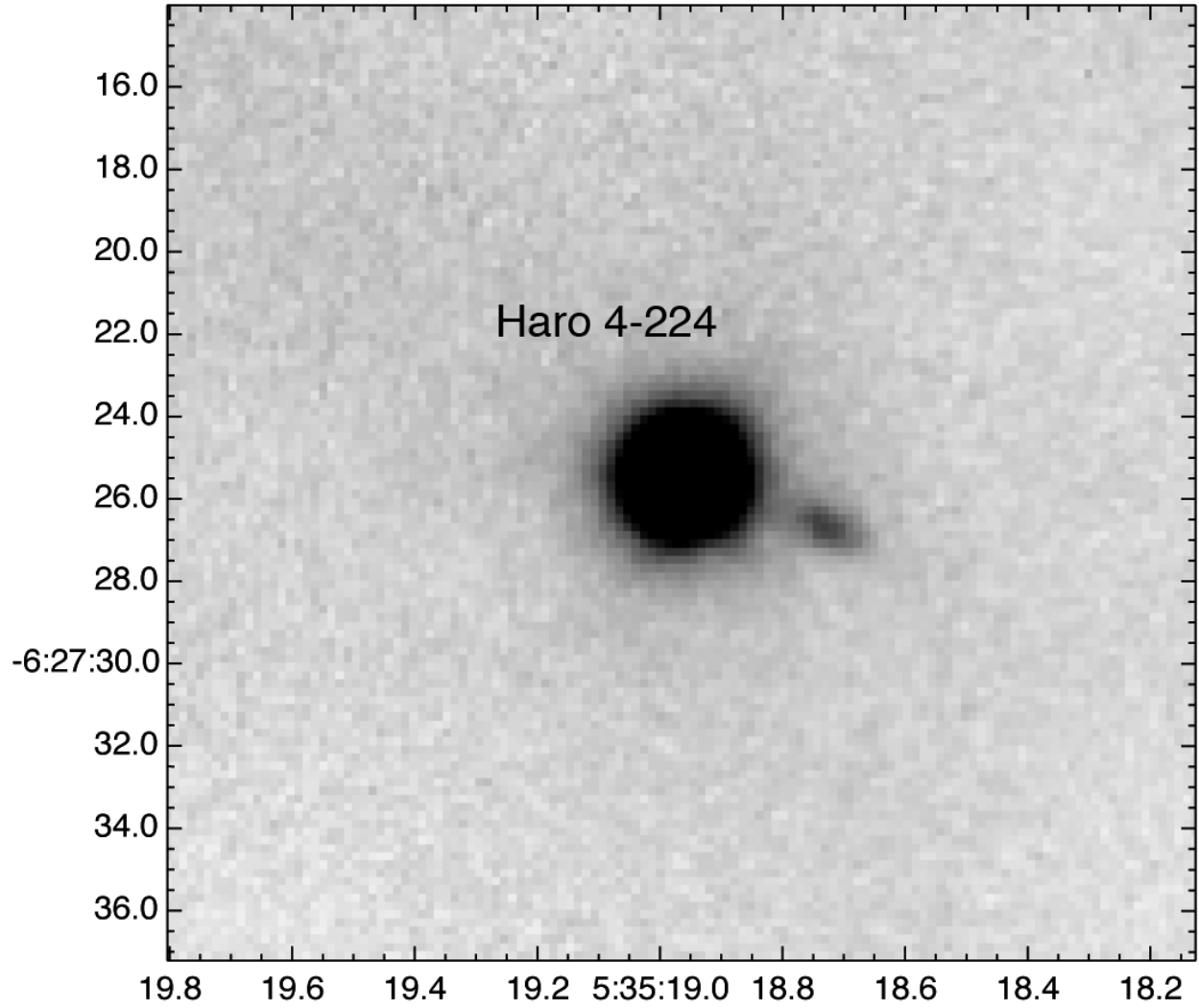


Fig. 4.— The HH 1022 jet emanating from the young star Haro 4-224 as seen in a [SII] image from the Subaru 8m telescope.

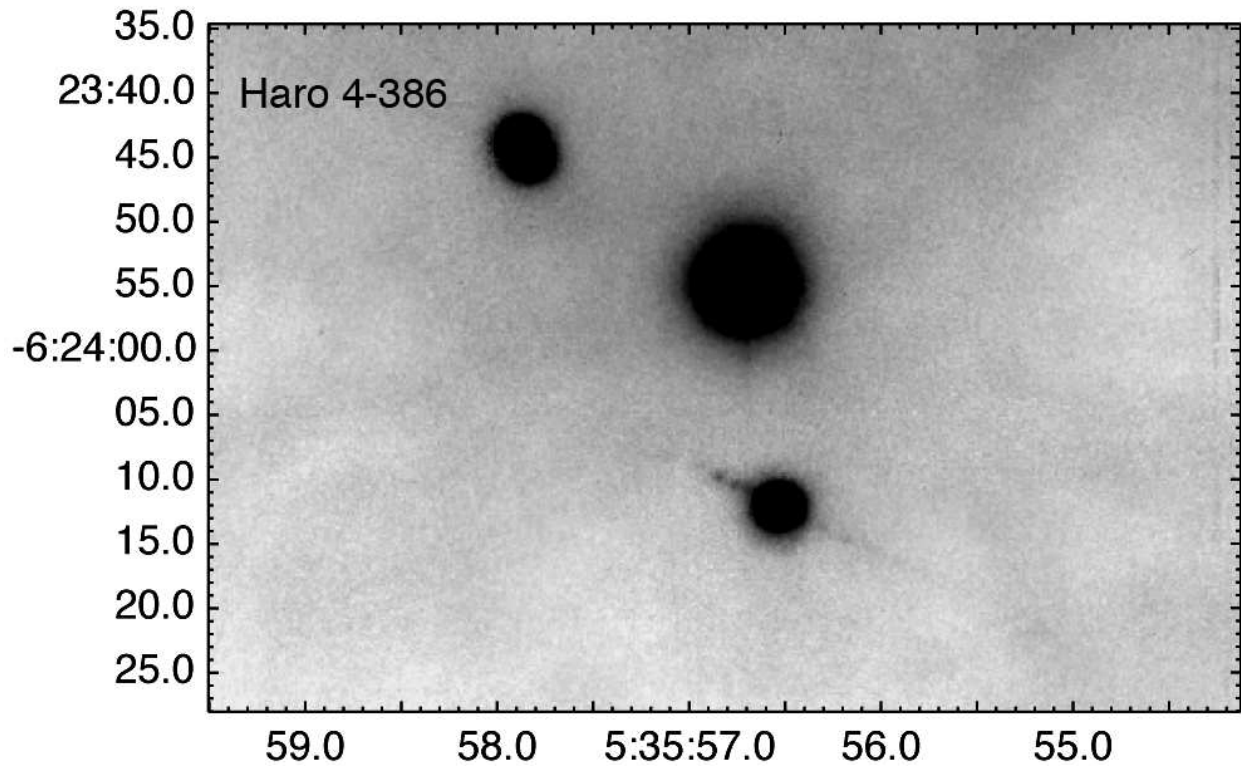


Fig. 5.— The HH 1023 jet emanating from 2MASS J05355651-0624122 as seen in an  $H\alpha+[SII]$  image from the Subaru 8m telescope.

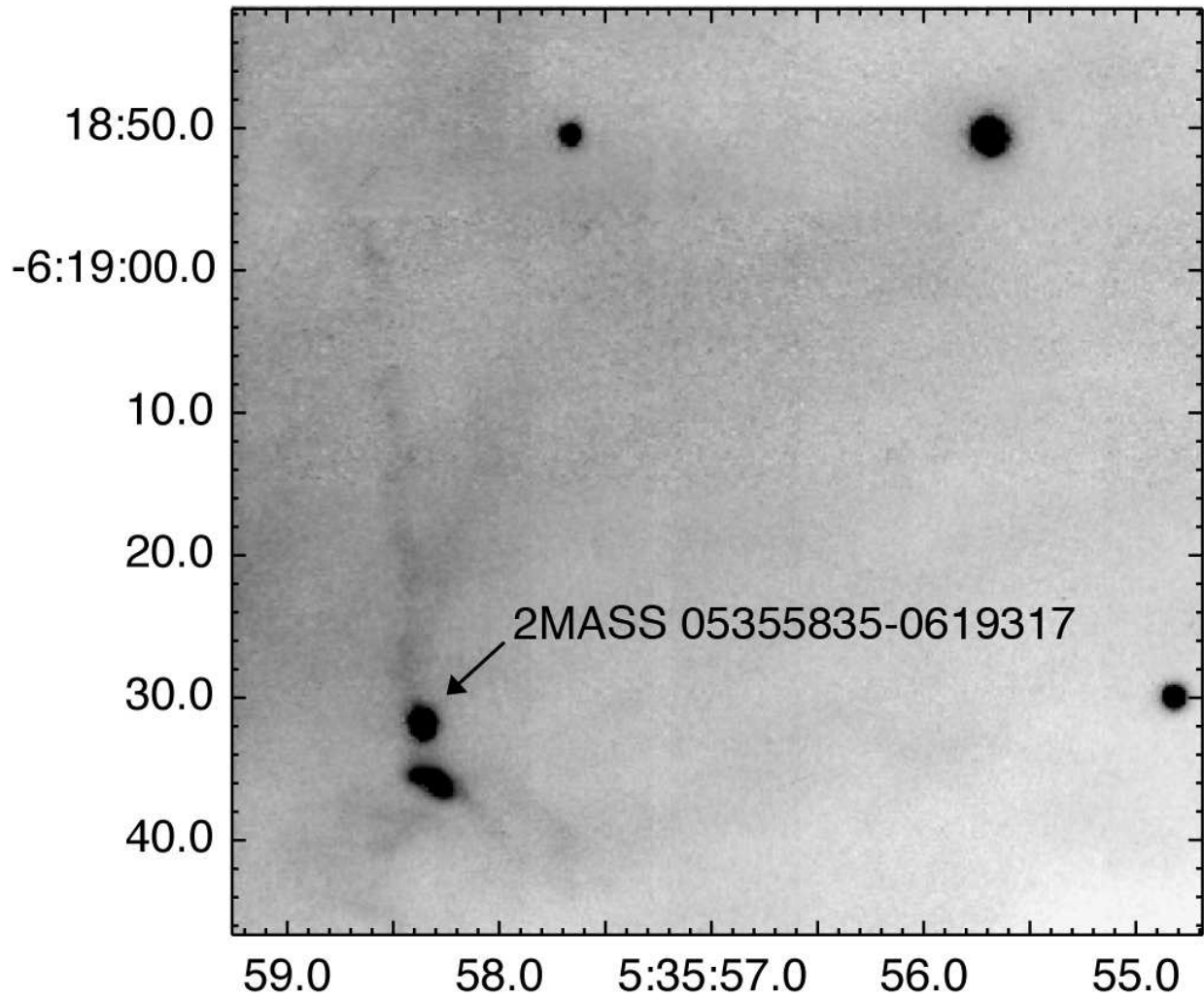


Fig. 6.— The HH 1024 jet emanating from 2MASS J05355835-0619317 as seen in an H $\alpha$  image from the Subaru 8m telescope.

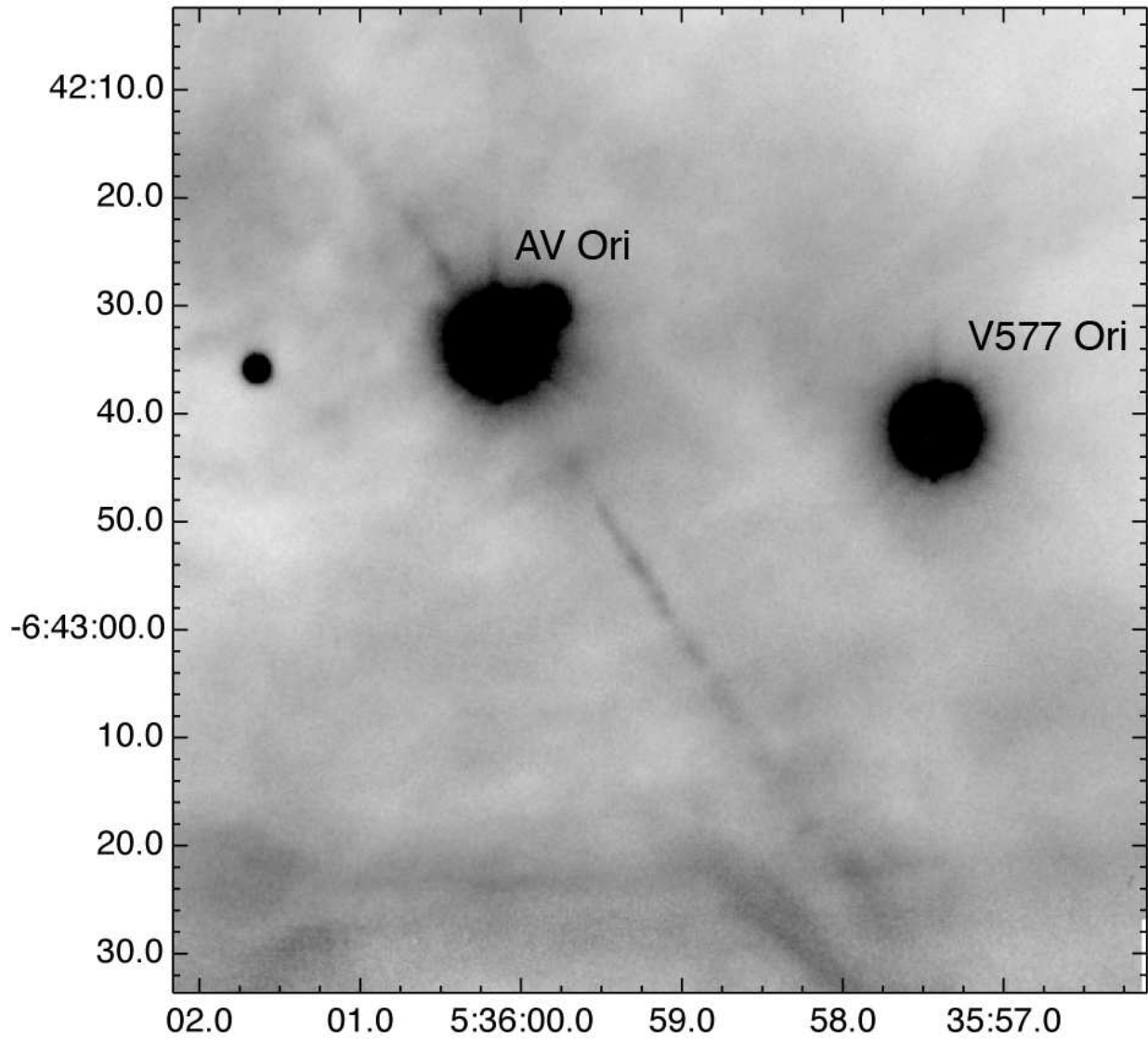


Fig. 7.— The HH 1025 jet emanating from AV Ori as seen in an  $H\alpha+[SII]$  image from the Subaru 8m telescope.

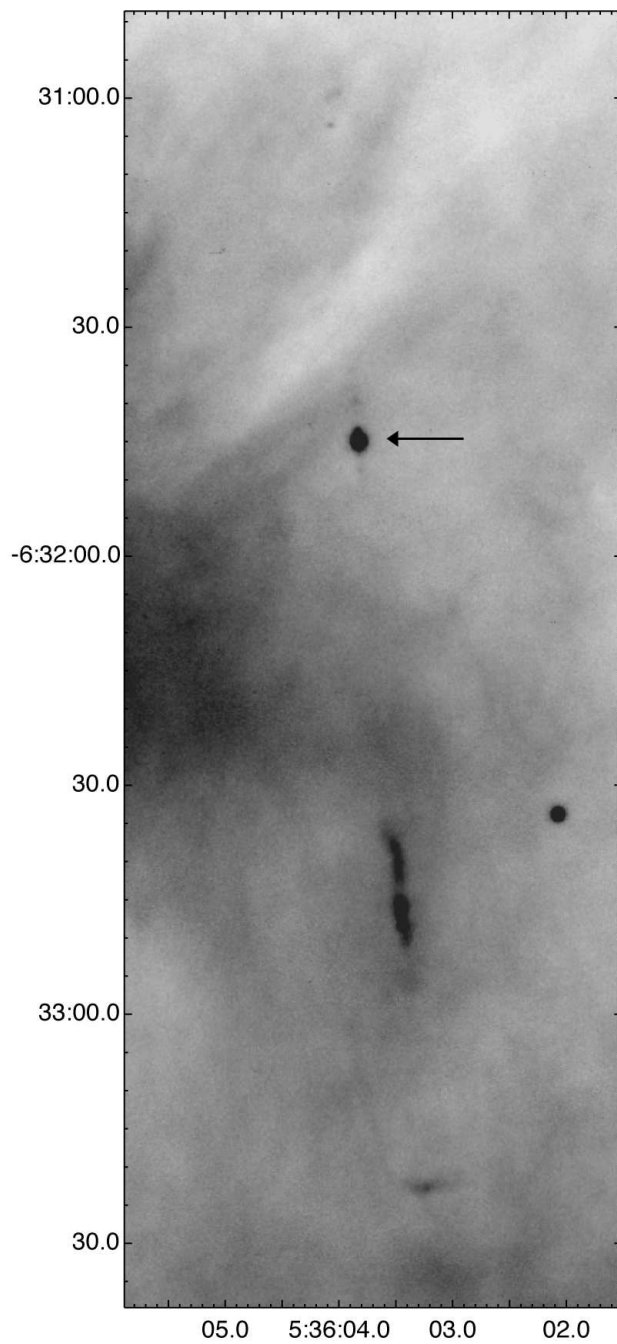


Fig. 8.— The HH 1026 jet emanating from an anonymous source as seen in an  $H\alpha+[SII]$  image from the Subaru 8m telescope. The arrow points at the driving source.

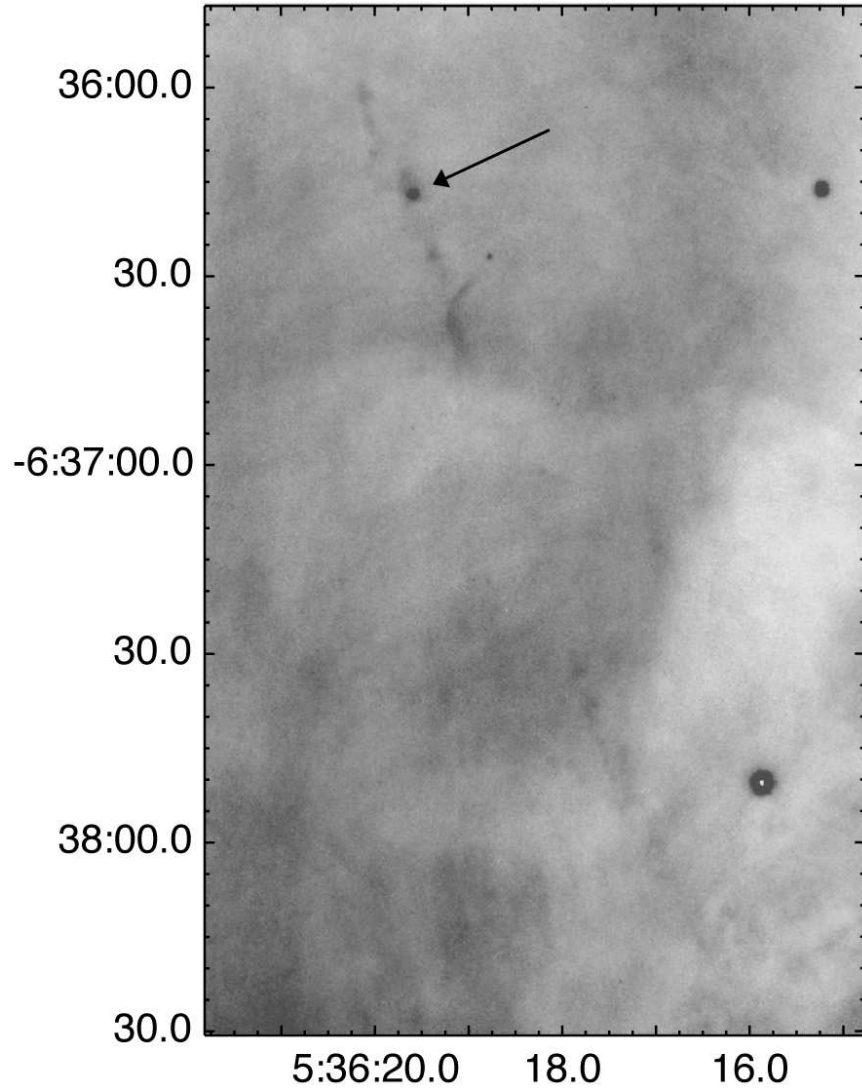


Fig. 9.— The HH 1027 jet emanating from 2MASS J05361960-0636171 as seen in a [SII] image from the Subaru 8m telescope. The arrow points at the driving source.

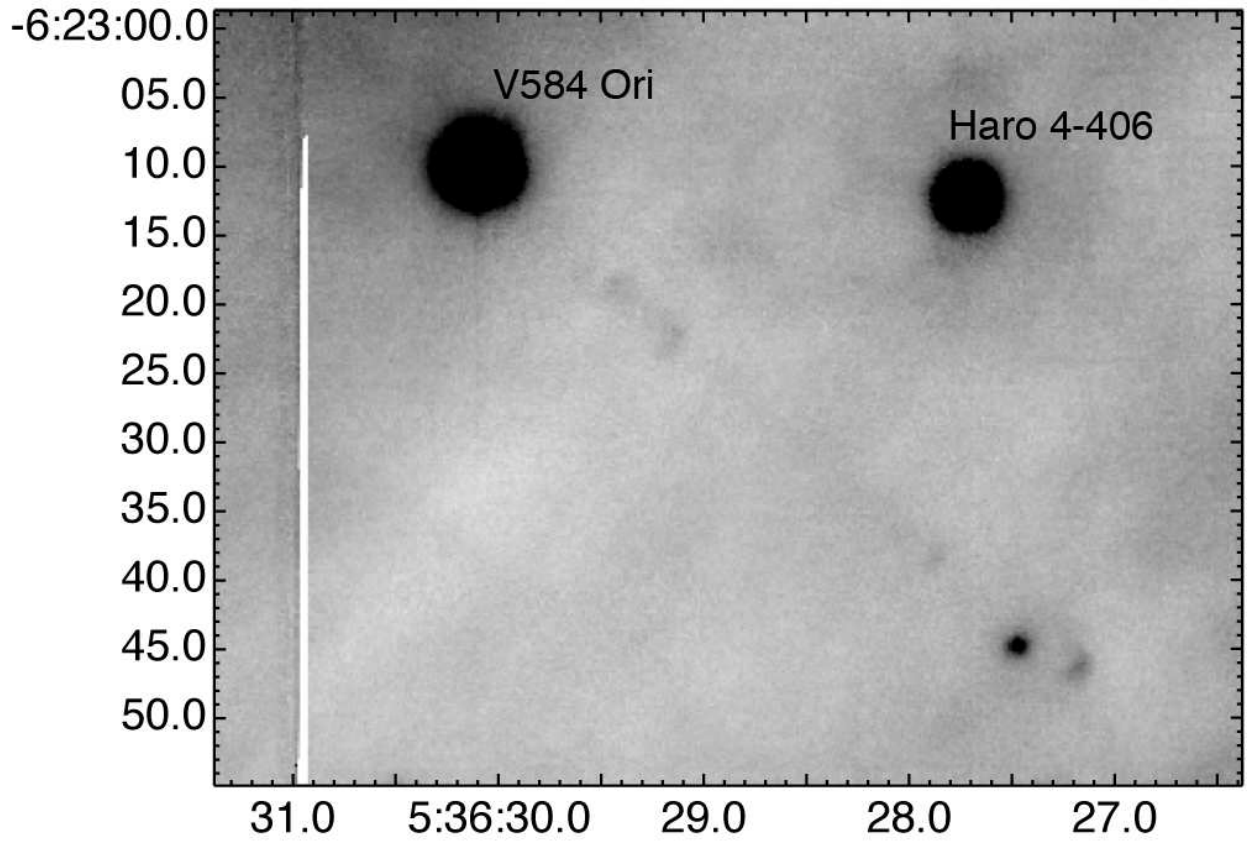


Fig. 10.— The HH 1028 jet emanating from V584 Ori as seen in an  $H\alpha + [SII]$  image from the Subaru 8m telescope. The two brightest knots at the lower right are both strong in  $[SII]$  emission, while the fainter knots mainly emit in  $H\alpha$ .

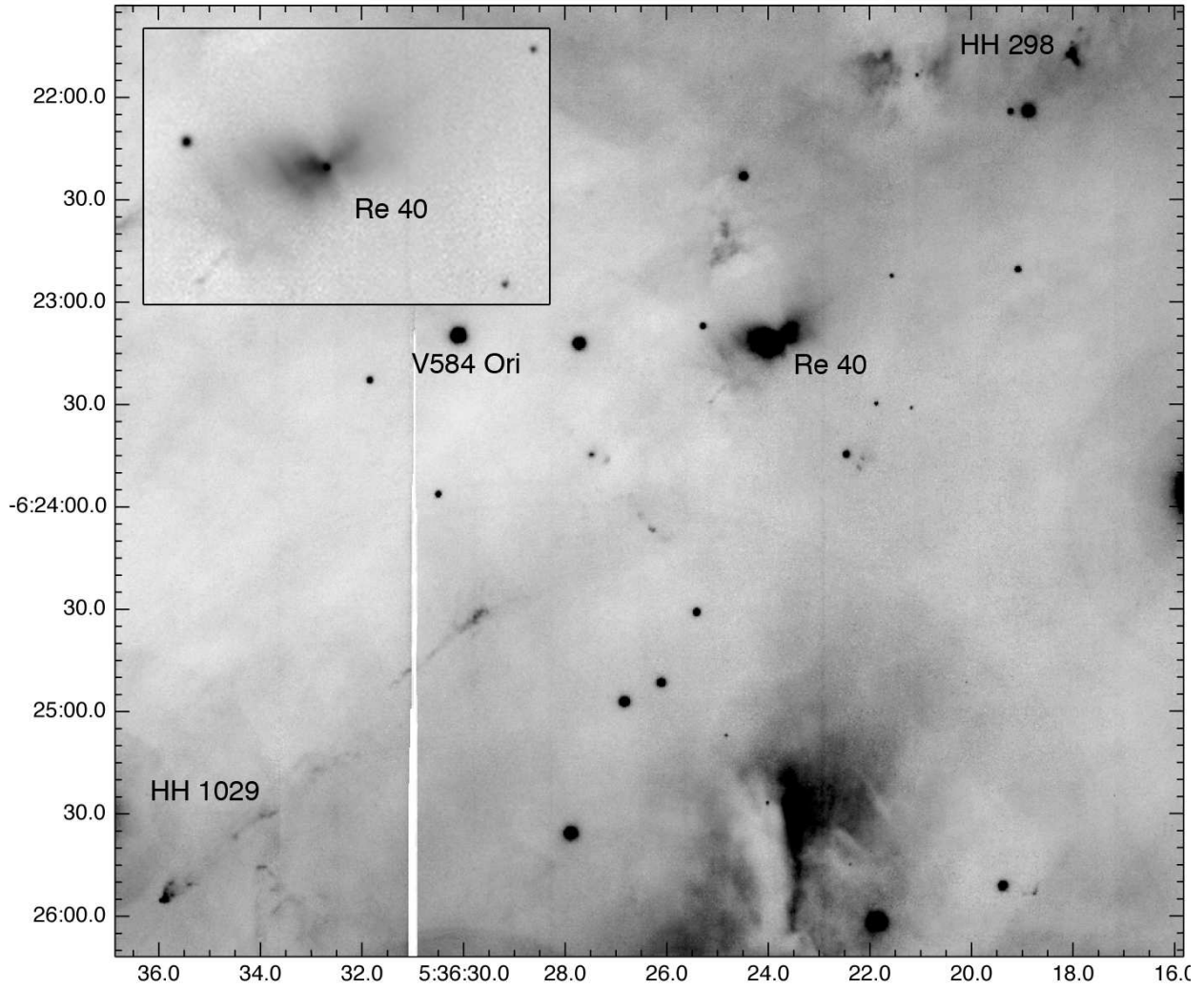


Fig. 11.— The HH 1029 is a jet emanating from a nebulous star south of the L1641-N cluster. The figure shows a [SII] image of the region, and is 5' wide, with north up and east left. Charge overflow from a bright star below the image crosses the figure. The insert shows an enlargement with a different intensity cut of the nebulous driving source Re 40 with its disk shadow and its two very faint, highly collimated jets. The HH 1028 jet (see previous figure) is at right angles to the HH 1029 flow.

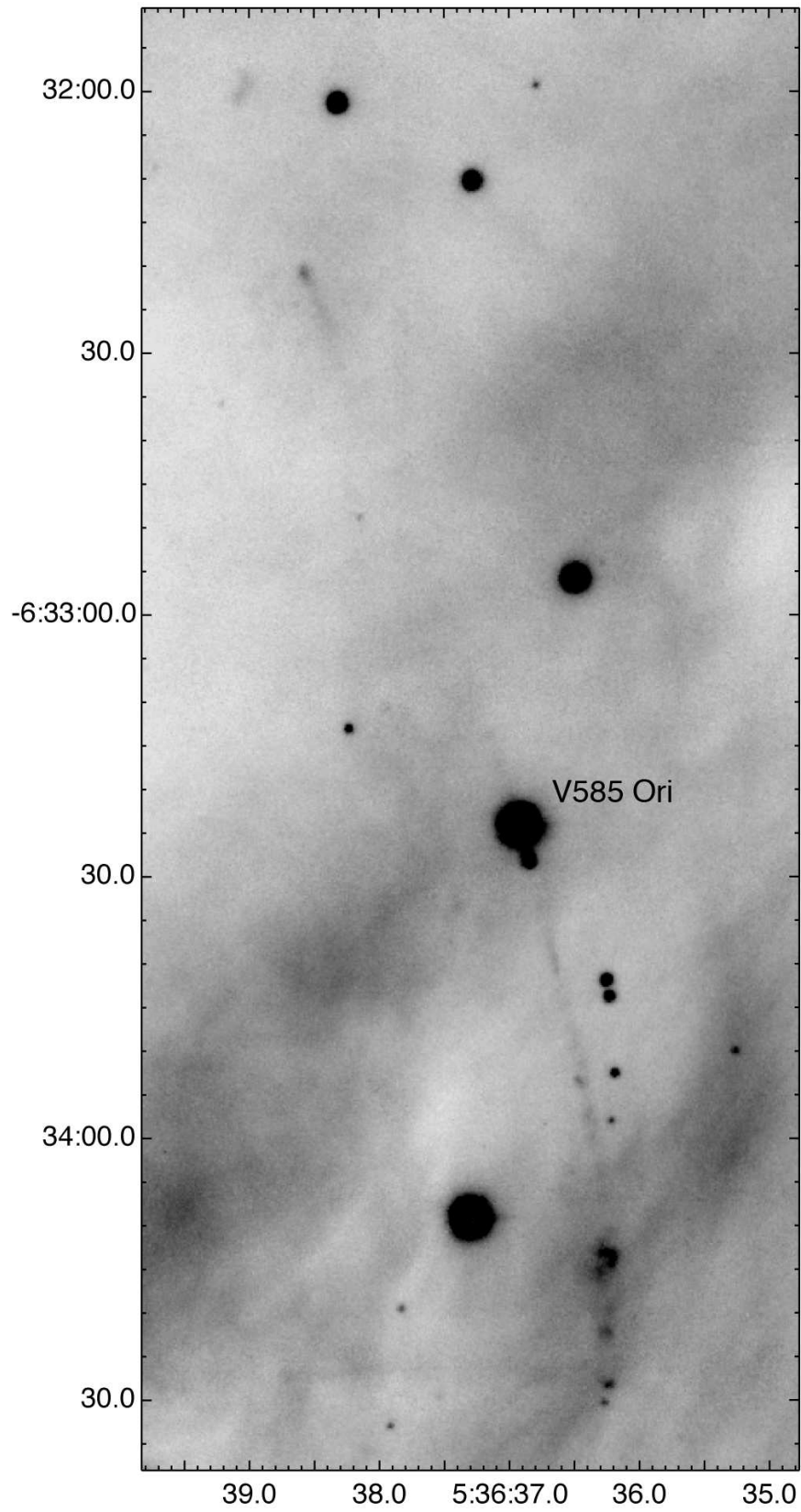


Fig. 12.— The HH 1030 jet emanating from V585 Ori as seen in an  $H\alpha + [SII]$  image from the Subaru 8m telescope.

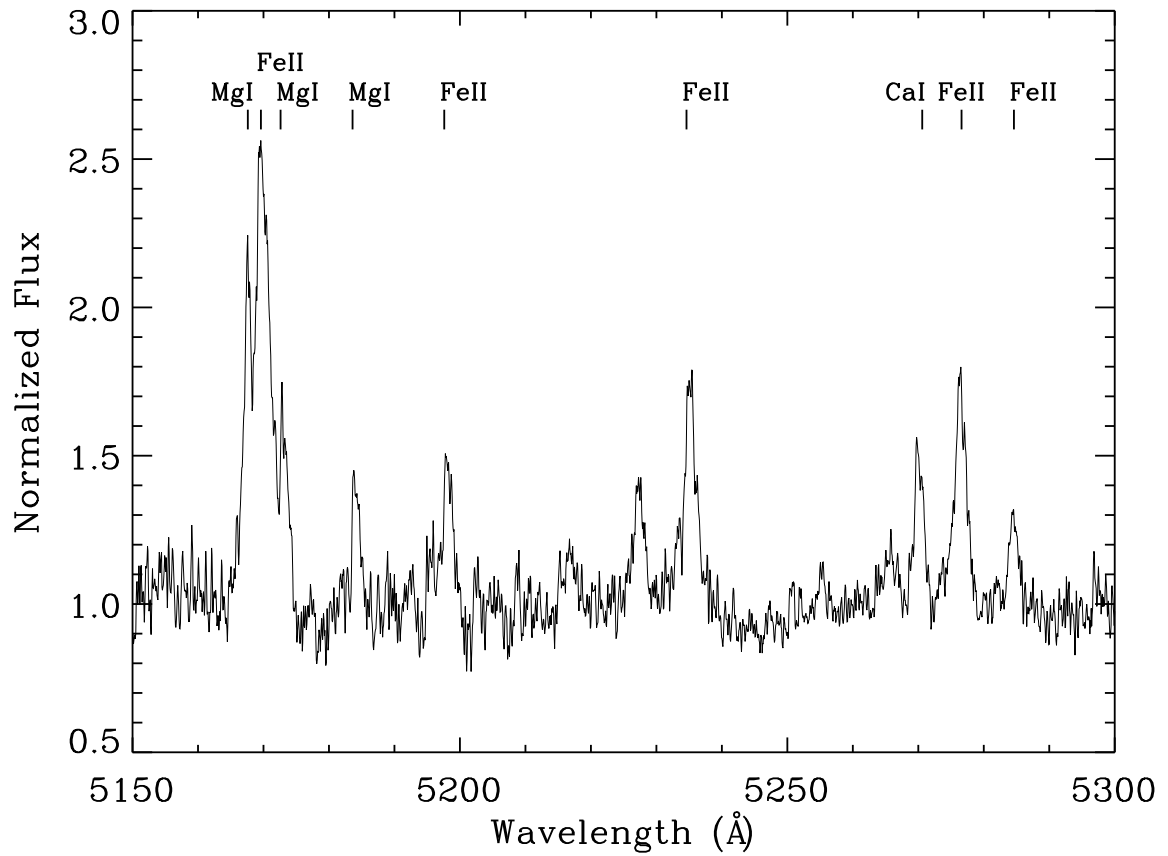


Fig. 13.— A Hectochelle spectrum of HH 1030 IRS = V585 Ori in the 5150 – 5300 Å region reveals a rich emission line spectrum.

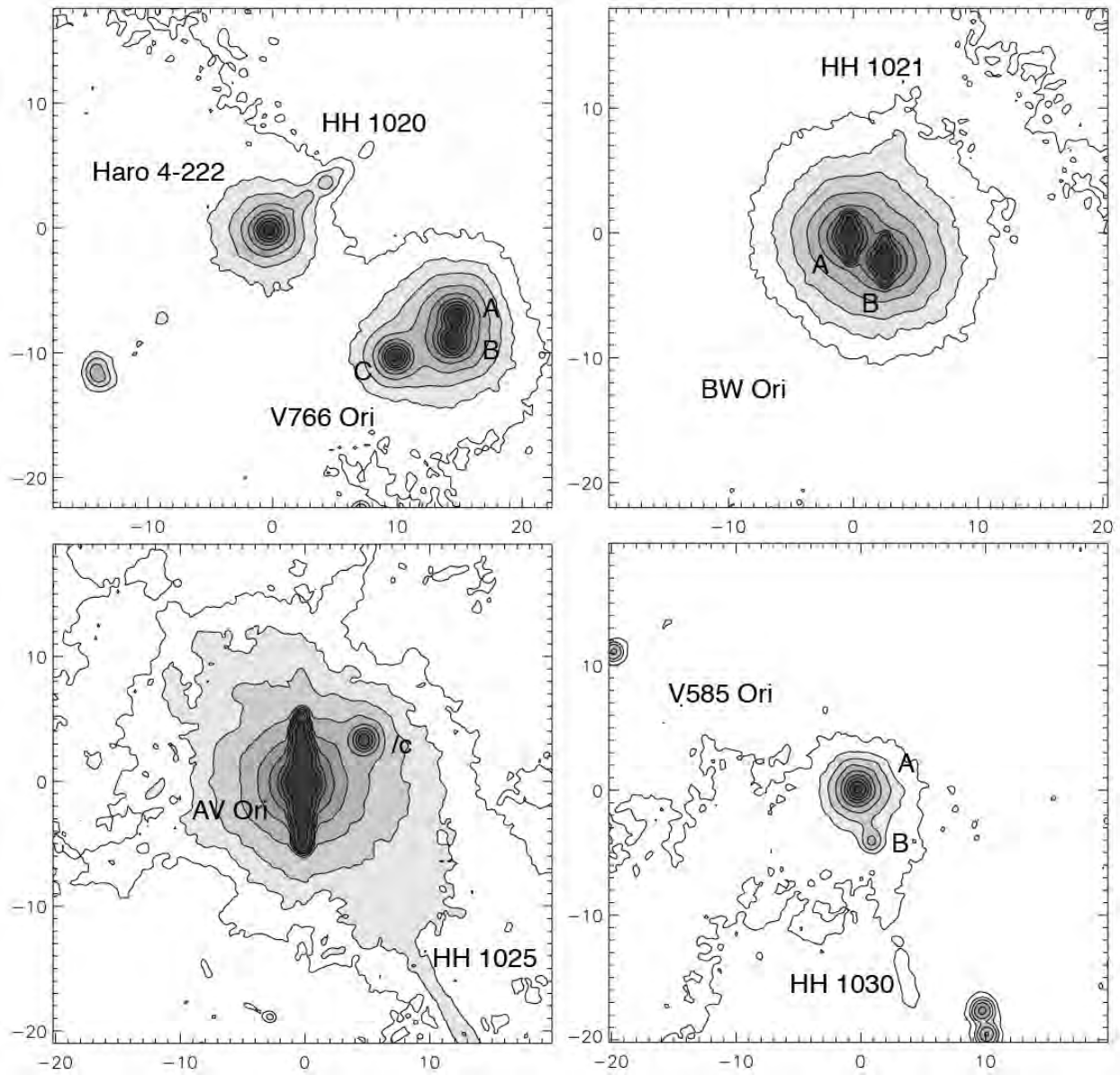


Fig. 14.— Contourplots of the four binary or multiple systems among the 11 jet sources, based on the [SII] image. Tickmarks are in arcseconds.

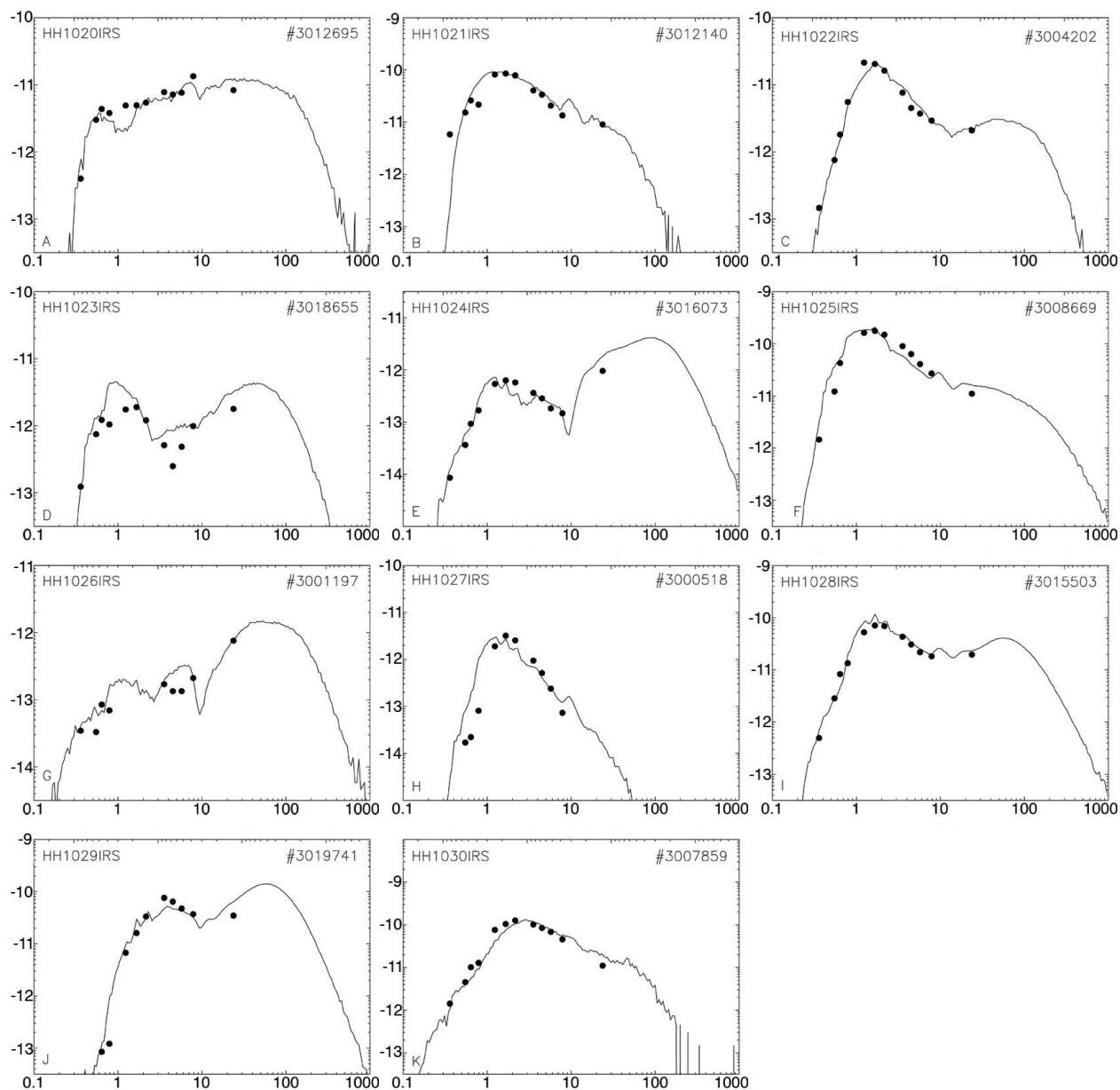


Fig. 15.— Spectral energy distributions of the 11 jet sources using SDSS, 2MASS, and Spitzer photometry modeled with the Robitaille et al. (2007) models. Beyond the longest-wavelength data points the models are unconstrained, and therefore more uncertain. The number in the upper right corner is the Robitaille et al. model identification. See text for details.

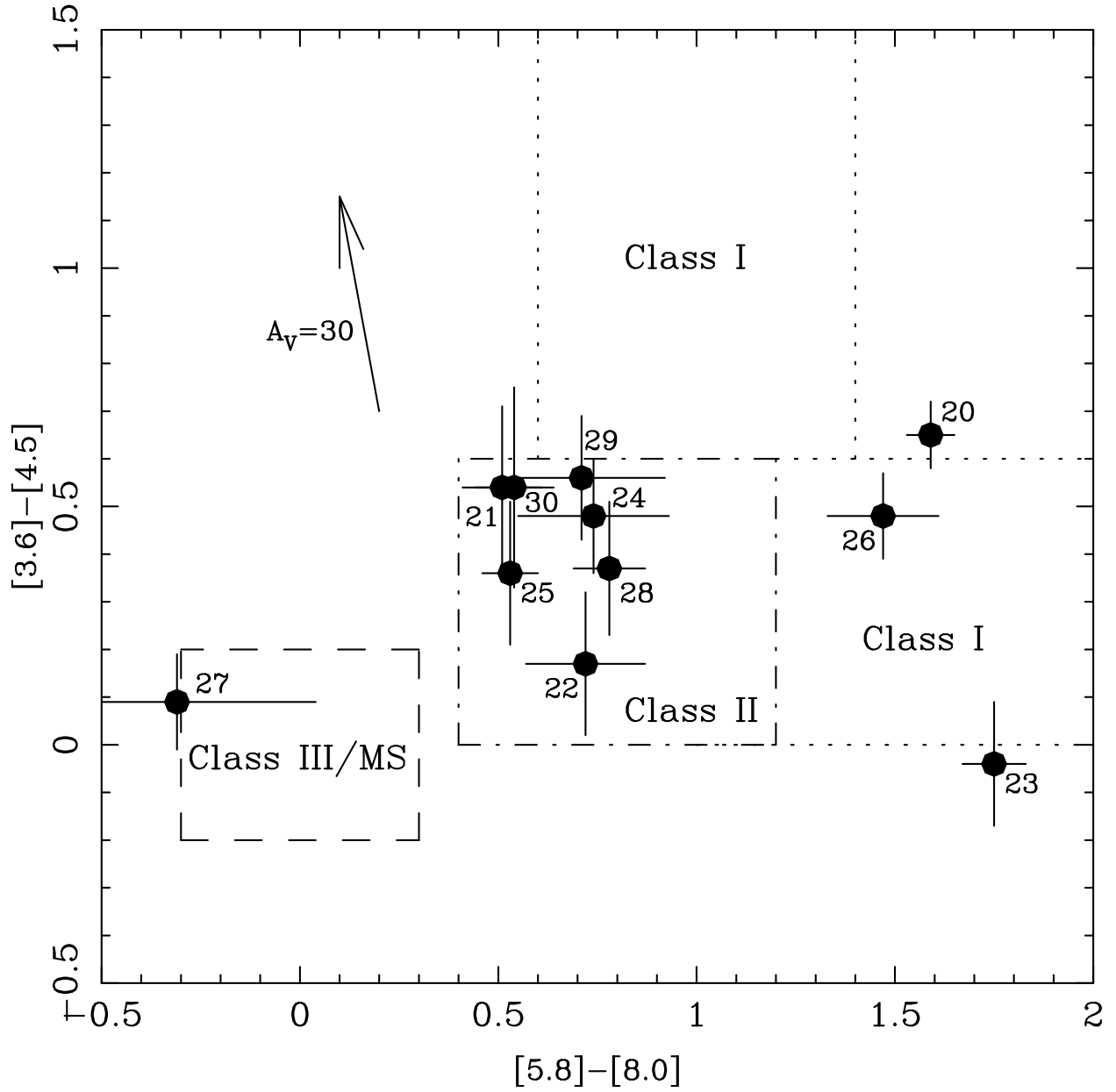


Fig. 16.— A color-color diagram from Spitzer IRAC photometry showing the location of the new jet sources relative to different classes of young stars. The boxes are from Allen et al. (2004). The numbers are the last two digits in the HH number for the associated outflows.

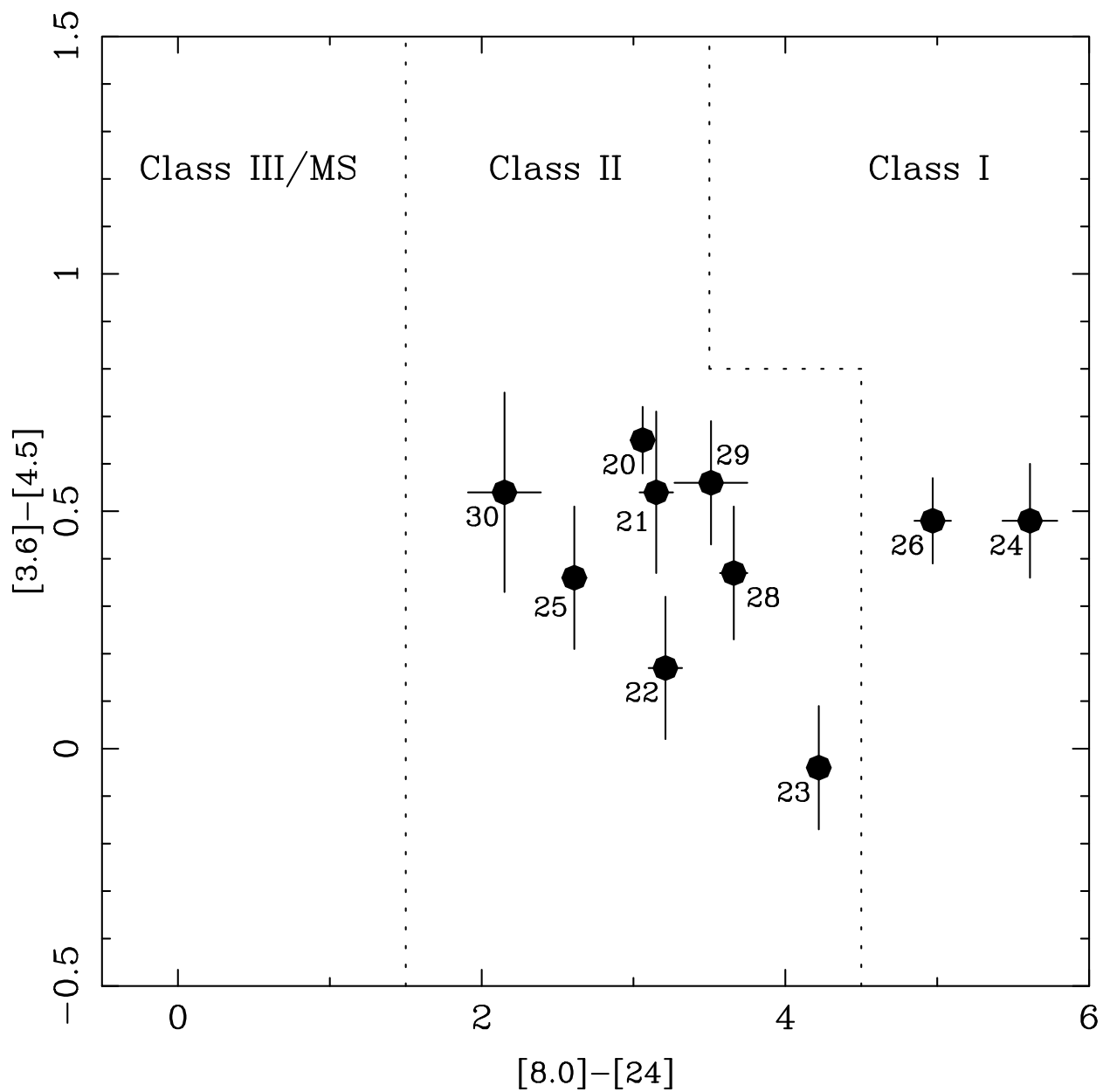


Fig. 17.— A color-color diagram from Spitzer MIPS photometry showing the location of the new jet sources relative to different classes of young stars. The boxes are from Balog et al. (2007). The driving source of HH 1027 is not detected at  $24 \mu\text{m}$  and is not included here. The numbers are the last two digits in the HH number for the associated outflows.

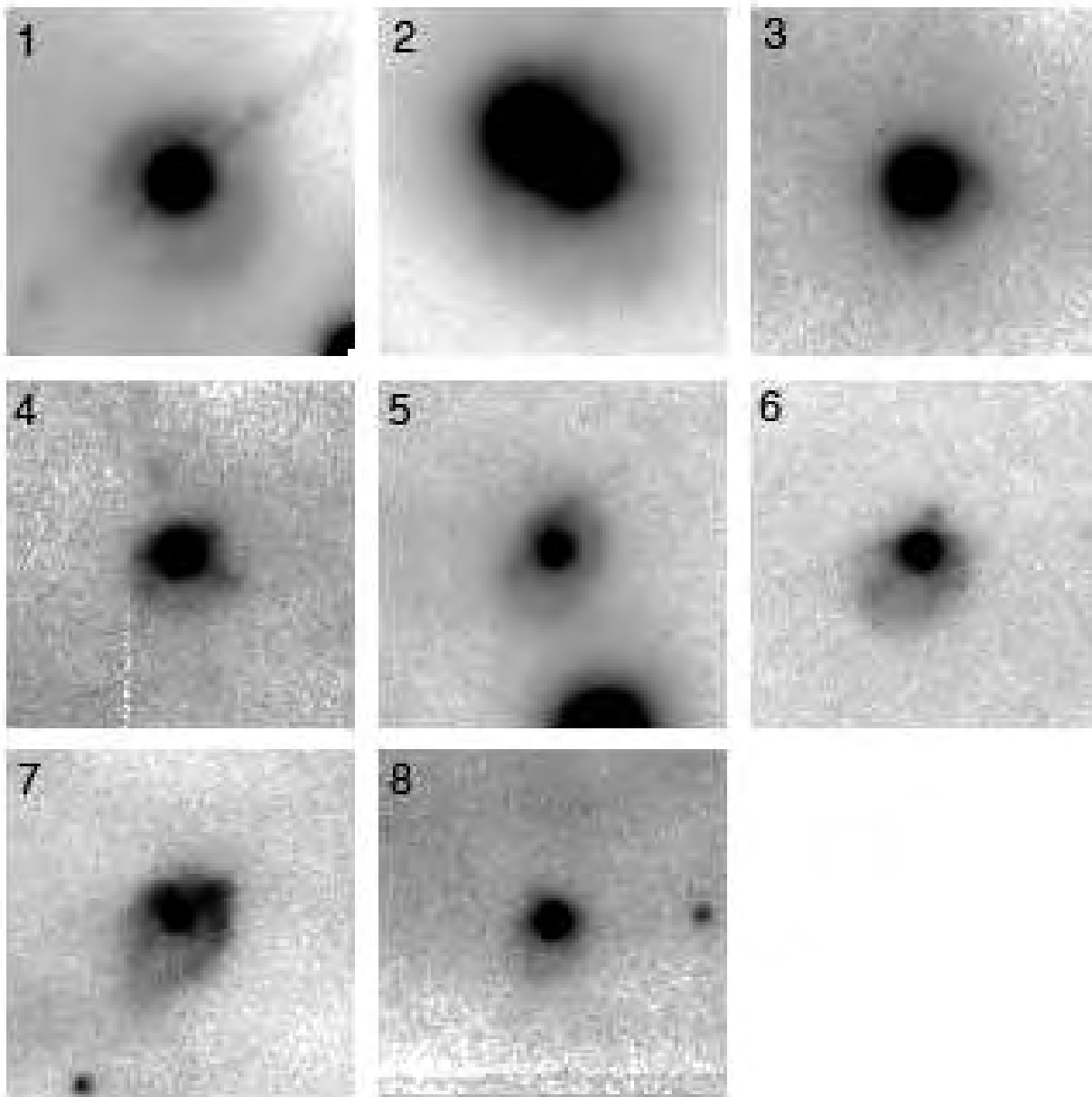


Fig. 18.— Faint H $\alpha$  emission envelopes surround 8 young stars in the regions studied here. Numbers refer to Table 4. Each stamp is  $15 \times 15$  arcseconds. North is up and east is left.

Table 1. Coordinates and Identifications of Jet Sources in Northern L1641.

Source	2MASS	Other Id	$\alpha_{2000}$	$\delta_{2000}$	Comments
HH 1020 IRS	05343988-0625140	Haro 4-222	5 34 39.9	–6 25 14	Trapezium
HH 1021 IRS	05345404-0623507	BW Ori	5 34 54.0	–6 23 51	Double
HH 1022 IRS	05351894-0627255	Haro 4-224	5 35 18.9	–6 27 26	
HH 1023 IRS	05355651-0624122		5 35 56.5	–6 24 12	
HH 1024 IRS	05355835-0619317		5 35 58.4	–6 19 32	
HH 1025 IRS	05360017-0642339	AV Ori	5 36 00.2	–6 42 34	Double
HH 1026 IRS			5 36 03.8	–6 31 45	
HH 1027 IRS	05361960-0636171		5 36 19.6	–6 36 17	
HH 1028 IRS	05363009-0623101	V584 Ori	5 36 30.1	–6 23 10	
HH 1029 IRS	05362378-0623113	Haro 4-403	5 36 23.8	–6 23 11	Edge-on disk
HH 1030 IRS	05363692-0633241	V585 Ori	5 36 36.9	–6 33 24	Double

Table 2. Radial Velocities of Selected Jet Sources.

Source	$V_{hel}$	$\Delta V_{hel}$	$R^a$	Comments
HH 1020 IRS	13.7	1.0	17.6	possible spectroscopic binary
HH 1021 IRS	23.1	0.4	8.8	good fit, narrow emission lines
HH 1022 IRS	20.6	1.3	10.1	good fit
HH 1023 IRS	35.4	2.1	5.7	faint, clear peak in correlation
HH 1028 IRS	26.6	0.5	28.7	good fit
HH 1030 IRS	25.4	3.0	–	fit to emission lines

<sup>a</sup>Cross correlation parameter

Table 3. Photometry of Jet Sources in Northern L1641.

Filter	1020	1021	1022	1023	1024	1025	1026	1027	1028	1029	1030
$u^a$	18.95	16.04	20.04	20.22	23.12	17.54	21.61		18.72		17.57
	.02	.01	.06	.05	.75	.01	.45		.01		.01
$g^a$	17.09	15.33	18.59	18.60	21.88	15.57	21.99	22.71	17.15	22.12	16.64
	.01	.01	.01	.01	.11	.01	.11	.58	.01	.11	.01
$r^a$	16.25	14.31	17.20	17.63	20.43	13.77	20.53	21.98	15.55	20.52	15.33
	.01	.01	.01	.01	.03	.01	.05	.28	.01	.05	.01
$i^a$	16.05	14.16	15.64	17.45	19.44		20.40	20.23	14.68	19.79	14.73
	.01	.01	.01	.01	.02		.06	.07	.01	.04	.01
$z^a$	15.90	13.19	14.73	17.31	18.45	13.04	19.53	18.67	14.02	19.12	13.88
	.01	.01	.01	.01	.03	.01	.12	.05	.01	.09	.01
$J^b$	14.74	11.69	13.14	15.86	17.14	10.94		15.77	12.17	14.40	11.77
	.04	.08	.03	.07	.20	.03		.06	.03	.09	.03
$H^b$	13.93	10.84	12.39	14.97	16.17	10.05		14.40	11.04	12.65	10.62
	.04	.08	.03	.07	.22	.03		.05	.03	.07	.03
$K^b$	13.08	10.18	11.89	14.71	15.52	9.48		13.90	10.32	11.11	9.66
	.03	.05	.02	.08	.16	.02		.04	.02	.03	.02
$3.6^c$	11.21	9.42	11.23	14.16	14.54	8.55	15.36	13.50	9.35	8.74	8.42
	.05	.16	.11	.07	.09	.13	.08	.08	.11	.10	.17
$4.5^c$	10.56	8.88	11.06	14.20	14.06	8.19	14.88	13.42	8.98	8.18	7.88
	.05	.03	.10	.11	.05	.06	.03	.04	.08	.07	.08
$5.8^c$	9.74	8.66	10.52	12.73	13.79	7.92	14.13	13.50	8.60	7.76	7.36
	.04	.06	.06	.07	.10	.04	.10	.21	.06	.05	.05
$8.0^c$	8.15	8.15	9.80	10.98	13.05	7.39	12.66	13.81	7.82	7.05	6.82
	.04	.08	.06	.04	.15	.05	.10	.33	.05	.20	.05
$24^d$	5.09	5.00	6.59	6.76	7.44	4.78	7.69		4.16	3.54	4.78
	.07	.08	.05	.03	.05	.06	.05		.06	.10	.07

<sup>a</sup>SDSS courtesy Min Fang

<sup>b</sup>2MASS

<sup>c</sup>Spitzer IRAC

<sup>d</sup>Spitzer MIPS

Table 4.  $H\alpha$  Envelopes in Northern L1641.

No.	$\alpha_{2000}$	$\delta_{2000}$	Diameter	PA	Source	Jet	Comments
1	05 34 39.9	−06 25 14	5''	22	Haro 4-222	HH 1020	
2	05 34 54.0	−06 23 53	8''	10	BW Ori	HH 1021	
3	05 35 18.9	−06 27 25	3''	30	Haro 4-224	HH 1022	
4	05 35 23.2	−06 23 37	3''	15		Faint $H\alpha$ knot to PA 15?	
5	05 35 27.4	−06 19 31	1.5'' $\times$ 3''	330			elongated
6	05 35 37.6	−06 38 56	3''	320			elongated
7	05 35 38.1	−06 42 34	2''				
8	05 35 50.6	−06 40 31	2'' $\times$ 4''	335			teardrop-shaped